ARTICLE

Untangling the contribution of Haspin and Bub1 to Aurora B function during mitosis

Michael A. Hadders* , Sanne Hindriksen*, My Anh Truong , Aditya N. Mhaskar, J. Pepijn Wopken, Martijn J.M. Vromans , and Susanne M.A. Lens

Aurora B kinase is essential for faithful chromosome segregation during mitosis. During (pro)metaphase, Aurora B is concentrated at the inner centromere by the kinases Haspin and Bub1. However, how Haspin and Bub1 collaborate to control Aurora B activity at centromeres remains unclear. Here, we show that either Haspin or Bub1 activity is sufficient to recruit Aurora B to a distinct chromosomal locus. Moreover, we identified a small, Bub1 kinase–dependent Aurora B pool that supported faithful chromosome segregation in otherwise unchallenged cells. Joined inhibition of Haspin and Bub1 activities fully abolished Aurora B accumulation at centromeres. While this impaired the correction of erroneous KT–MT attachments, it did not compromise the mitotic checkpoint, nor the phosphorylation of the Aurora B kinetochore substrates Hec1, Dsn1, and Knl1. This suggests that Aurora B substrates at the kinetochore are not phosphorylated by centromere-localized pools of Aurora B, and calls for a reevaluation of the current spatial models for how tension affects Aurora B–dependent kinetochore phosphorylation.

Introduction

To maintain genomic integrity during mitosis, the duplicated chromosomes need to be correctly distributed over the two daughter cells. This requires that sister chromatids become connected to microtubules emanating from opposing poles of the mitotic spindle (amphitelic attachment). Microtubules attach to chromosomes via specialized protein structures called kinetochores, which assemble on centromeres (Musacchio and Desai, 2017). Formation of correct, amphitelic attachments of kinetochore microtubules (kMTs) is facilitated by a dynamic kinetochore–microtubule interface (KT–MT) that allows the detachment of improper connections such as syntelic attachments (both kinetochores attached to microtubules from the same mitotic spindle pole) or merotelic attachments (one kinetochore attached to microtubules from both sides of the mitotic spindle), and the stabilization of amphitelic attachments. A key player in this "error correction" process is the chromosomal passenger complex (CPC), consisting of Aurora B kinase, IN-CENP, Survivin, and Borealin. Aurora B destabilizes KT–MT attachments by phosphorylating several outer kinetochore proteins that directly bind microtubules, including components of the Knl1/Mis12 complex/Ndc80 complex (KMN) network (Cheeseman et al., 2006; Cimini et al., 2006; DeLuca et al., 2006; Tanaka et al., 2002; Welburn et al., 2010). Destabilization of KT–MT attachments transiently generates unattached kinetochores, which provide the sister chromatids with another

opportunity to be captured by microtubules. Additionally, unattached kinetochores activate the mitotic checkpoint, a surveillance mechanism that prevents the onset of anaphase until all kinetochores have become attached to microtubules of the mitotic spindle (Foley and Kapoor, 2013; Lampson and Cheeseman, 2011). Aurora B also feeds into the mitotic checkpoint in a more direct way by facilitating the rapid recruitment of the essential checkpoint kinase Mps1 to kinetochores (Santaguida et al., 2011; Saurin et al., 2011) and by phosphorylating the kinetochore protein Knl1. Phosphorylation of Knl1 prevents the binding of PP1γ, the phosphatase that counteracts Mps1-dependent phosphorylation of Knl1 (Liu et al., 2010; Nijenhuis et al., 2014). Thus, Aurora B contributes to faithful chromosome segregation by facilitating error correction and mitotic checkpoint maintenance.

During the early stages of mitosis, Aurora B is predominantly observed at the inner centromere, a specialized region on the chromatin that lies at the intersection of the inter-kinetochore axis and the inter-sister chromatid axis (Hindriksen et al., 2017a; Yamagishi et al., 2010). The typical inner centromere localization of Aurora B is considered important for its activity toward substrates at the outer kinetochore: it concentrates Aurora B kinase in proximity of these substrates, while at the same time allowing spatial regulation of kinetochore substrate phosphorylation (Andrews et al., 2004; Krenn and Musacchio, 2015; Liu

....

et al., 2009; Tanaka et al., 2002; Wang et al., 2011; Welburn et al., 2010).

Two evolutionarily conserved kinases, Haspin and Bub1, direct the docking of the CPC to the inner centromere. The cohesin-associated kinase Haspin phosphorylates histone H3 on threonine 3 (H3T3ph), and H3T3ph directly interacts with the CPC via Survivin (Dai et al., 2005; Du et al., 2012; Jeyaprakash et al., 2011; Kelly et al., 2010; Niedzialkowska et al., 2012; Wang et al., 2010; Yamagishi et al., 2010). The kinetochore-localized kinase Bub1 phosphorylates (centromeric) histone H2A on threonine 120 (H2AT120ph). H2AT120ph recruits the paralogs Shugoshin 1 and Shugoshin 2 (Sgo1/2), which in turn bind to the CPC subunit Borealin (Kawashima et al., 2007, 2010; Liu et al., 2015; Tsukahara et al., 2010; Yamagishi et al., 2010). The prevailing model is that the CPC is recruited to the chromatin region where H3T3ph and H2AT120ph overlap (Yamagishi et al., 2010), implying that the CPC inner centromere confinement may be defined by simultaneous interactions of the CPC with H3T3ph and Sgo1/2 that localize to H2AT120ph (Krenn and Musacchio, 2015; Trivedi and Stukenberg, 2016). However, the two histone marks do not evidently overlap: H3T3ph appears as a single dot at the inner centromere, while H2AT120ph can be observed as two foci that are in closer proximity to the kinetochore (Liu et al., 2013; Yamagishi et al., 2010). This led us to hypothesize that instead of converging to accumulate the CPC precisely at the inner centromere, Haspin and Bub1 might each recruit a separate functional CPC pool to the centromere (Fig. 1 A). Indeed, we demonstrate that Haspin or Bub1 kinase activity can individually recruit Aurora B to an ectopic chromosomal locus. Furthermore, a detailed analysis of HCT116 Haspin CRISPR mutant (CM) cells revealed a small, Bub1-dependent Aurora B pool that was sufficient for faithful chromosome segregation in otherwise unchallenged cells. Inhibition of Bub1 in Haspin CM cells abolished accumulation of Aurora B in the centromere region, and while this increased the frequency of anaphases with lagging chromosomes, it surprisingly did not compromise the mitotic checkpoint, or the phosphorylation of the Aurora B kinetochore substrates Dsn1, Hec1, and Knl1. Our findings suggest that the correction of erroneous KT–MT attachments is more sensitive to reductions in centromeric Aurora B levels than activation of the mitotic checkpoint and the phosphorylation of the tested kinetochore substrates.

Results

Haspin and Bub1 kinase individually recruit Aurora B to an ectopic locus

We hypothesized that Haspin and Bub1 might each localize a functional CPC pool near the centromere, instead of collectively creating a local environment where the CPC makes simultaneous interactions with H3T3ph and H2AT120ph, in case of the latter most likely via Sgo1/2 (Fig. 1 A; Tsukahara et al., 2010; Yamagishi et al., 2010). To discriminate between these possibilities, while excluding effects of cross-talk between the different proteins, we made use of U-2 OS-LacO cells, which harbor an array of lac operator repeats on chromosome 1 (Janicki et al., 2004). Expression of Haspin or Bub1 fused to LacI-GFP allowed
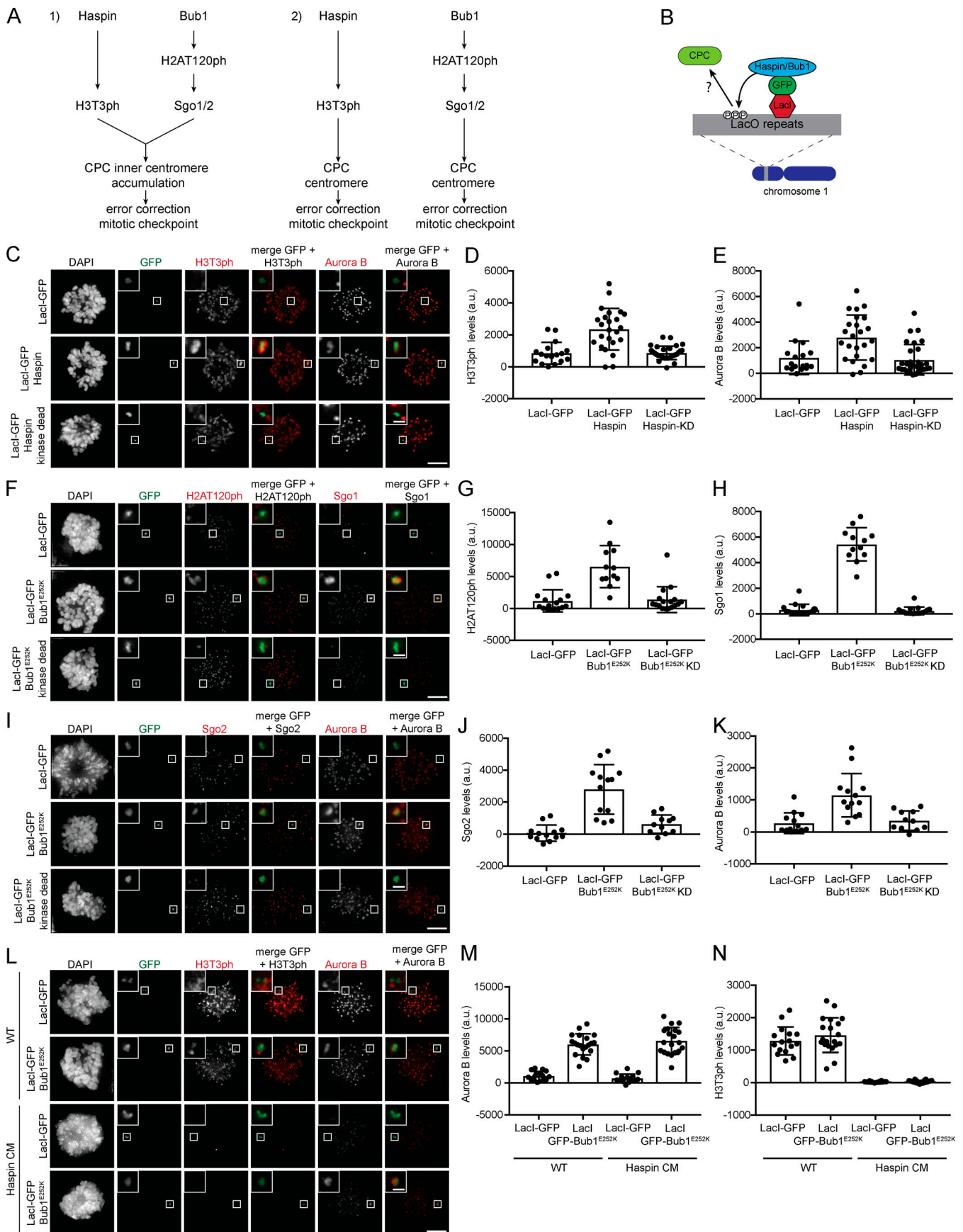
us to assess CPC recruitment to the ectopic LacO locus by each individual kinase (Fig. 1 B). As readout for CPC recruitment, we measured Aurora B levels using quantitative immunofluorescence (IF) microscopy. Expression of LacI-GFP-Haspin in U-2 OS-LacO cells resulted in local phosphorylation of H3T3 and in the recruitment of Aurora B, in contrast to cells expressing LacI-GFP (Fig. 1, C–E; and Fig. S1 A). Aurora B recruitment required Haspin kinase activity, because expression of a kinase dead mutant of Haspin did not result in H3T3ph signal at the LacO locus or in Aurora B recruitment (Fig. 1, C–E; and Fig. S1 A).

To study the capacity of Bub1 to recruit the CPC, we used a LacI-GFP-Bub1 fusion protein harboring a mutation in its GLEBS domain (E252K, hereafter called LacI-GFP-Bub1^{E252K}; Fig. S1, B and C; Krenn et al., 2012; Overlack et al., 2015; Ricke et al., 2012). Bub1 recruitment to the kinetochore protein Knl1 depends on the interaction of its GLEBS domain with Bub3 (Larsen et al., 2007; Primorac et al., 2013; Taylor et al., 1998). The use of Bub1^{E252K} excluded recruitment of kinetochore proteins to the LacO locus, which we observed when expressing WT LacI-GFP-Bub1 (Fig. S1, D–H). In contrast to LacI-GFP, ectopic localization of LacI-GFP-Bub1^{E252K} resulted in local phosphorylation of H2AT120 and recruitment of Sgo1, Sgo2, and Aurora B, which was not observed upon ectopic targeting of a kinase dead mutant of Bub1^{E252K} (Fig. 1, F–K; and Fig. S1, B and C). Since Bub1 is thought to recruit the CPC via Sgo1/2 (Kawashima et al., 2007, 2010; Tsukahara et al., 2010), we bypassed Bub1 and expressed either Sgo1-LacI-GFP or LacI-GFP-Sgo2. Indeed, both LacI fusion proteins recruited Aurora B to the LacO array (Fig. S1, I–K).

To exclude the possibility that endogenous Bub1 kinase activity contributed to Aurora B recruitment by ectopically localized Haspin, we analyzed Aurora B recruitment by LacI-GFP-Haspin in cells depleted of Bub1 using siRNA (Fig. S1, L–O). Transfection of siBub1 abolished chromatin-associated H2AT120ph, indicating that Bub1 depletion was successful (Fig. S1, L and N). In the absence of phosphorylated H2AT120, LacI-GFP-Haspin could still recruit Aurora B to the LacO array (Fig. S1, L–O). To analyze if Aurora B recruitment by Bub1 could occur independently of Haspin activity, we mutated the endogenous Haspin gene in U-2 OS-LacO cells using CRISPR/Cas9 (U-2 OS-LacO Haspin CM; Table S1). While H3T3 was no longer phosphorylated in these cells, expression of LacI-GFP-Bub1^{E252K} was still capable of recruiting Aurora B to the LacO array (Fig. 1, L–N; and Fig. S1, P and Q). These data show that either Haspin or Bub1 activity is sufficient to recruit Aurora B to an ectopic locus.

Loss of Haspin kinase activity reveals a Bub1 kinase–dependent Aurora B pool at centromeres

Next, we performed a detailed analysis of Aurora B localization in cells in the absence of Haspin and/or Bub1 kinase activity, to investigate if Haspin and Bub1 could also recruit separate pools of the CPC to centromeres. We generated two Haspin mutants in HCT116 cells using CRISPR/Cas9, each generated with a unique single guide RNA (sgRNA) targeting GSG2 (the gene encoding Haspin). The first gRNA targets GSG2 just before the kinase domain at position bp 1306–1308, yielding Haspin CM1, while the second gRNA targets the start of GSG2, at position bp 39–41, hereafter called Haspin CM2. In each cell line, both Haspin

Hadders et al.
Multiple functional pools of Aurora B

Journal of Cell Biology 2 of 20
https://doi.org/10.1083/jcb.201907087

Hadders et al.
Multiple functional pools of Aurora B

Journal of Cell Biology   3 of 20
https://doi.org/10.1083/jcb.201907087

Figure 1.   **Haspin and Bub1 kinase activities independently recruit Aurora B to an ectopic locus. (A)** Models for how Haspin and Bub1 may mediate centromeric recruitment of the CPC. **(B)** Schematic depiction of the assay used to test the ability of LacI-GFP-Haspin or LacI-GFP-Bub1 to recruit the CPC to a LacO-array. **(C, F, and I)** IF images of U-2 OS-LacO cells expressing the indicated LacI-GFP fusion proteins and arrested in prometaphase using STLC (scale bar, 5 µm). The insets show the magnification of the boxed region (scale bar, 1 µm). IF intensity levels of H3T3ph (D), Aurora B (E), H2AT120ph (G), Sgo1 (H), Sgo2 (J), and Aurora B (K) at the LacO-array were quantified. The graphs show quantifications from individual cells (dots) and the mean (bar) ± SD. A minimum of 17 cells (D and E) or 11 cells (G, H, J, and K) was quantified per condition. Data are representative of two independent experiments, with the exception of the IF for Sgo2 (J), which was performed once. **(L)** IF images of U-2 OS-LacO and U-2 OS-LacO Haspin CM cells expressing LacI-GFP or LacI-GFP-Bub1[E252K]. Cells were arrested in prometaphase using STLC (scale bar, 5 µm). The insets show the magnification of the boxed region (scale bar 1 µm). **(M)** IF intensity levels of Aurora B levels at the LacO-array. **(N)** IF intensity levels of H3T3ph on the DNA. The graphs show quantifications from individual cells (dots) and the mean (bar) ± SD. A minimum of 16 cells was quantified per condition. Data are representative of three independent experiments.

alleles were mutated, resulting in premature stop codons (Table S1). Loss of Haspin activity was further confirmed by the lack of H3T3ph detected by Western blot and by IF imaging (Fig. S2, A, B, and D). Compared with WT HCT116 cells, centromeric levels of Aurora B were reduced by ∼50% in the Haspin CM cell lines (Fig. 2, A and C; and Fig. S2, A and C). Interestingly, chromosome spreads consistently revealed two kinetochore-proximal foci of Aurora B in the Haspin CM cells, similar to previous observations for Borealin in cells treated with the Haspin inhibitor 5-ITu (Bekier et al., 2015; Fig. 2, D and F). Because Haspin also helps to maintain centromeric cohesin (Dai et al., 2006, 2009; Liang et al., 2018; Zhou et al., 2017), it was unclear if the two Aurora B foci represented an alternative CPC pool, or reflected separated sister centromeres caused by weakened cohesion. Measurements of CENP-C/CENP-C distances in these chromosome spreads showed that on average, inter-kinetochore distances were increased in the Haspin CM cells as compared with WT cells (Fig. 2, D and E). However, even on chromosomes with CENP-C/CENP-C distances comparable to WT cells (552 nm), Aurora B was observed as two kinetochore-proximal foci in the Haspin CM cells (556 nm, Fig. 2, D-F). In WT HCT116 cells, Aurora B was mainly localized to the inner centromere, even on chromosomes with larger inter-kinetochore distances (Fig. 2, D and F). Interestingly, in WT cells, a small kinetochore-proximal pool of Aurora B was also observed, in addition to the main inner centromere pool (Fig. 2, D and F). These observations implied that the kinetochore-proximal Aurora B localization in Haspin CM cells most likely represents an alternative pool of the CPC, distinct from that at the inner centromere. Because of its localization, proximal to the kinetochore, we hypothesized this pool of Aurora B may depend on Bub1 activity. Indeed, inhibition of Bub1 kinase activity using the small molecule inhibitor BAY-320 (Baron et al., 2016) abolished this pool of Aurora B in Haspin CM cells (Fig. 2, A–D). This suggests that Bub1 activity can recruit a small, kinetochore-proximal pool of Aurora B to centromeres independently of Haspin.

Of note, we chose to inhibit Bub1 kinase activity instead of depleting Bub1, because Bub1 also has nonenzymatic functions, including the recruitment of mitotic checkpoint proteins to the kinetochore, a function that is maintained after inhibition of its kinase activity (Baron et al., 2016; Meraldi and Sorger, 2005; Raaijmakers et al., 2018; Rodriguez-Rodriguez et al., 2018; Zhang et al., 2019). As previously reported, treatment of cells with the Bub1 inhibitor BAY-320 markedly reduced H2AT120ph and Sgo1 levels at the centromere (Fig. 2, A and B; and Fig. S2 E; Baron et al., 2016). Centromeric levels of Aurora B were reduced by

∼40% in cells treated with BAY-320 (Fig. 2, A and C). Inspection of chromosome spreads showed that in Bub1-inhibited cells, Aurora B localized along the inter-sister chromatid axis, although some enrichment in the inner centromere region was still visible (Fig. 2 D). While we cannot fully exclude that this is caused by residual Bub1 activity, the observed localization is similar to what has been reported for Bub1 knockdown in cell lines and for mouse embryonic fibroblasts derived from Bub1 kinase-dead mutant mice (Ricke et al., 2012; Yamagishi et al., 2010). The inter-sister chromatid and inner centromere pool of Aurora B, observed upon Bub1 inhibition in WT cells, is not observed when Bub1 is inhibited in Haspin CM cells, strongly suggesting that Haspin is responsible for the recruitment of this pool of Aurora B (Fig. 2, A and D). Bub1 inhibition in Haspin CM cells resulted in low levels of residual Aurora B, dispersed over the chromatin, and quantifications at the centromeres revealed a reduction in Aurora B levels of ∼70% (Fig. 2, A and C). Collectively, our data support the idea that Haspin and Bub1 can recruit separate pools of Aurora B to the inter-sister chromatid region and the kinetochore-proximal centromere, respectively, in early mitosis.

The Haspin- and Bub1-controlled pools of Aurora B support error-free chromosome segregation

To study the function of the two observed pools of the CPC during mitosis, we followed mitotic progression by live cell imaging using WT HCT116 or Haspin CM cells stably expressing H2B-mCherry. WT HCT116 and Haspin CM cells aligned their chromosomes on the metaphase plate with similar timing, and the incidence of chromosome segregation errors in anaphase in Haspin CM cells was comparable to WT cells (Fig. 3, A–C). Bub1 inhibition delayed anaphase onset by ∼10 min, due to a delay in chromosome congression (Fig. 3, B and C). Bub1 inhibition had only a minor effect on chromosome segregation fidelity (Fig. 3 A). This suggests that both the Aurora B pool controlled by Haspin and the pool controlled by Bub1 are largely capable of supporting faithful chromosome segregation. However, precluding centromeric accumulation of Aurora B, treatment of Haspin CM cells with BAY-320 caused a substantial increase in the fraction of cells with anaphase lagging chromosomes (Fig. 3 A). Importantly, the mitotic defects observed in Bub1-inhibited Haspin CM cells differed from the defects induced by Aurora B kinase inhibition. Inhibition of Aurora B with the small molecule inhibitor ZM447439 in WT HCT116 or Haspin CM cells severely disturbed chromosome alignment, and cells exited mitosis without discernable anaphases (Fig. 3, A and B), similar to
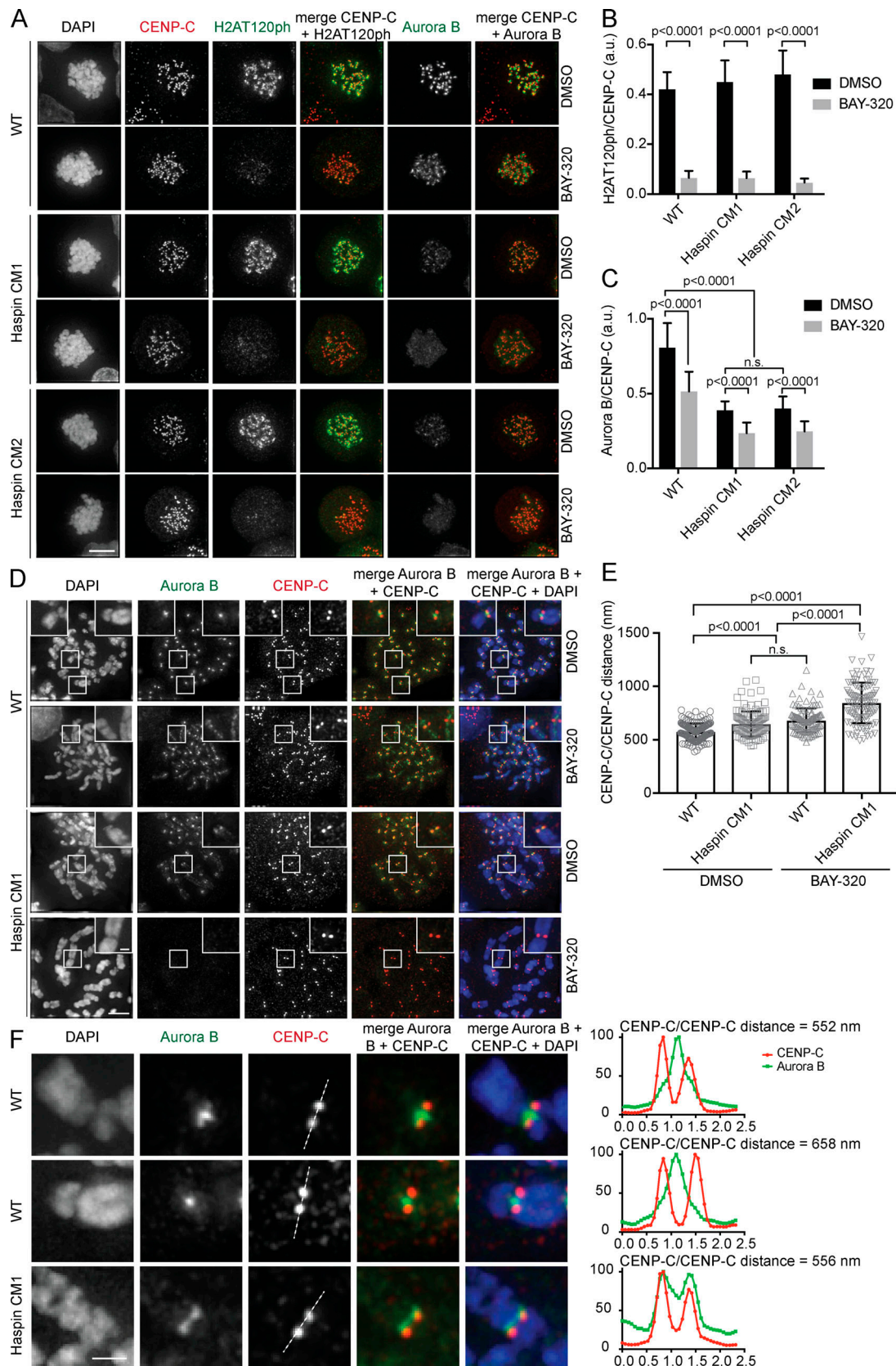
Figure 2. **Localization of Aurora B in HCT116 WT and Haspin CM cells with or without Bub1 inhibition. (A)** IF images of HCT116 WT or Haspin CM cells ±10 µM BAY-320 and arrested in mitosis using nocodazole (scale bar, 5 µm). **(B and C)** IF intensity levels of H2AT120ph (B) and Aurora B (C) at centromeres were quantified. Levels were normalized over CENP-C. The graphs show the mean and SD. A minimum of 25 cells was quantified per condition. Data are representative of two independent experiments. P values were calculated using a two-way ANOVA with Tukey's multiple comparison test. n.s., not significant.

Hadders et al.
Multiple functional pools of Aurora B

Journal of Cell Biology 5 of 20
https://doi.org/10.1083/jcb.201907087

(D) IF images of chromosome spreads prepared from HCT116 WT and Haspin CM cells ±10 µM BAY-320 (scale bar, 5 µm). The insets show the magnification of the boxed region (scale bar, 1 µm). **(E)** CENP-C/CENP-C distances from individual pairs of kinetochores (dots) and the mean (bar) and SD. A minimum of 103 kinetochore pairs was measured per condition. P values were calculated using a one-way ANOVA with Tukey's multiple comparison test. n.s., not significant. **(F)** Line plots depicting IF intensity levels of Aurora B and CENP-C, measured along a line that intersects the two sister CENP-C signals of the inter-kinetochore axis (scale bar, 1 µm). The Aurora B levels are normalized to the CENP-C signals. IF images of the specific kinetochore pairs represented in the line plots are shown on the left. The dotted lines in the CENP-C image correspond to the line plots.

previously reported effects of Aurora B inhibition in other cell lines (Cimini et al., 2006; Ditchfield et al., 2003; Girdler et al., 2008; Harrington et al., 2004; Hauf et al., 2003; Tao et al., 2008). This suggests that despite the lack of centromere-concentrated Aurora B in Bub1-inhibited Haspin CM cells, residual kinase activity limits the severity of chromosome bi-orientation and segregation errors.

### Haspin and Bub1 facilitate efficient Aurora B–dependent error correction

Our data suggest that the two Aurora B pools, controlled by either Haspin or Bub1, are largely redundant for faithful chromosome segregation during an otherwise unperturbed mitosis. However, error correction becomes more challenging when many faulty attachments are established early in mitosis (Ganem et al., 2009). Under these conditions, both Haspin and Bub1 might be required to accumulate sufficient amounts of active Aurora B at centromeres. To increase the frequency of erroneous KT–MT attachments, we inhibited Eg5 with monastrol to accumulate cells in mitosis with monopolar spindles (Kapoor et al., 2000; Khodjakov et al., 2003; Mayer et al., 1999). We then let cells progress through mitosis for a range of time points (from 45 to 180 min) after release from the monastrol block in the presence of the proteasome inhibitor MG132 to prevent anaphase onset (Lampson et al., 2004). The fraction of cells with fully aligned and misaligned chromosomes was scored and used as a proxy for error correction (Fig. 4, A and B). After 45 min, ±80% of WT cells had achieved full alignment, compared with ±49% for the Haspin CM cell lines (Fig. 4 B). After 90 min, WT cells reached maximal alignment (±91%). Importantly, Haspin CM cells largely recovered with ±81% and ±76% of cells showing complete alignment for Haspin CM1 and CM2, respectively. This suggests that Haspin CM cells are capable of correcting erroneous KT–MT attachments when given sufficient time. However, Haspin CM cells displayed a dramatic drop in the number of correct metaphases after 180 min with only ±25% of cells showing full chromosome alignment. Closer inspection of these cells revealed mainly chromosome scattering, as opposed to chromosome misalignment (Fig. 4 C). Since Haspin also contributes to maintenance of centromeric cohesion by locally blocking the activity of the cohesin removal factor WAPL (Dai et al., 2006; Liang et al., 2018; Zhou et al., 2017), we tested if depletion of WAPL could rescue the observed alignment defect in Haspin CM cells. Indeed, depletion of WAPL by siRNA transfection rescued chromosome alignment after 180 min but not after 60 min (Fig. 4, C–F), suggesting that the alignment defect observed early after the monastrol release is not a consequence of cohesin loss but due to impaired error correction.

We next studied the consequences of Bub1 inhibition on chromosome alignment in WT and Haspin CM cells, 60 min after monastrol release. The addition of BAY-320 did not affect chromosome alignment in WT cells; however, Bub1 inhibition exacerbated the alignment defect in Haspin CM cells, with only ±35% of cells reaching full alignment, compared with ±60% in Haspin CM cells. Moreover, depletion of WAPL was unable to rescue alignment (Fig. 4, E and F). To test if the congression defect observed in the Haspin CM cells plus Bub1 inhibition could recover when given more time to align, we also measured alignment after 3 h (Fig. S3 A). When Bub1 was inhibited in Haspin CM cells, it rendered the cells largely resistant against rescue by WAPL depletion, suggesting that the observed alignment defects were due to perturbed error correction and not loss of cohesion.

Taken together, our data show that Haspin loss only delays error correction, while the combined loss of Haspin and Bub1 activity severely compromises error correction. To test if the observed alignment defects after monastrol release were caused by the reduced centromeric Aurora B levels in Bub1-inhibited Haspin CM cells (Fig. 2, A and C), we expressed CENP-B (CB)–mCherry or CB-INCENP-mCherry in a doxycycline-inducible manner in HCT116 WT and Haspin CM cells (Huang et al., 2018; Liu et al., 2009; van der Waal et al., 2012). Addition of doxycycline restored centromeric Aurora B levels in CB-INCENP–expressing cells, in contrast to cells expressing CB-mCherry (Fig. S3, B and C). Expression of CB-INCENP but not CB-mCherry resulted in a near complete rescue of alignment in Bub-inhibited Haspin CM cells, with ±81% of cells reaching full alignment (Fig. 4 G). This suggests that the centromeric levels of Aurora B become the limiting factor for efficient error correction upon the concurrent loss of Haspin and Bub1 activity.

Phosphorylation of the Aurora B kinetochore substrates Hec1 and Dsn1 occurs in the absence of detectable centromere-concentrated Aurora B

While our data support the idea that Haspin and Bub1 recruit separate functional pools of Aurora B to centromeres, the mitotic defects observed in Bub1-inhibited Haspin CM cells were less severe than the defects induced by Aurora B kinase inhibition, suggesting residual Aurora B kinase activity in the absence of centromere concentrated Aurora B. Aurora B phosphorylates multiple kinetochore substrates in the KMN network, resulting in a dynamic KT–MT interface that facilitates correction of faulty microtubule attachments (Bakhoum et al., 2009b; DeLuca et al., 2011; Welburn et al., 2010; Zaytsev et al., 2016). We therefore performed quantitative IF for phosphorylated Hec1 (S44) and Dsn1 (S109), two Aurora B substrates of the KMN network (Kim and Yu, 2015; Welburn et al., 2010; Yang et al.,
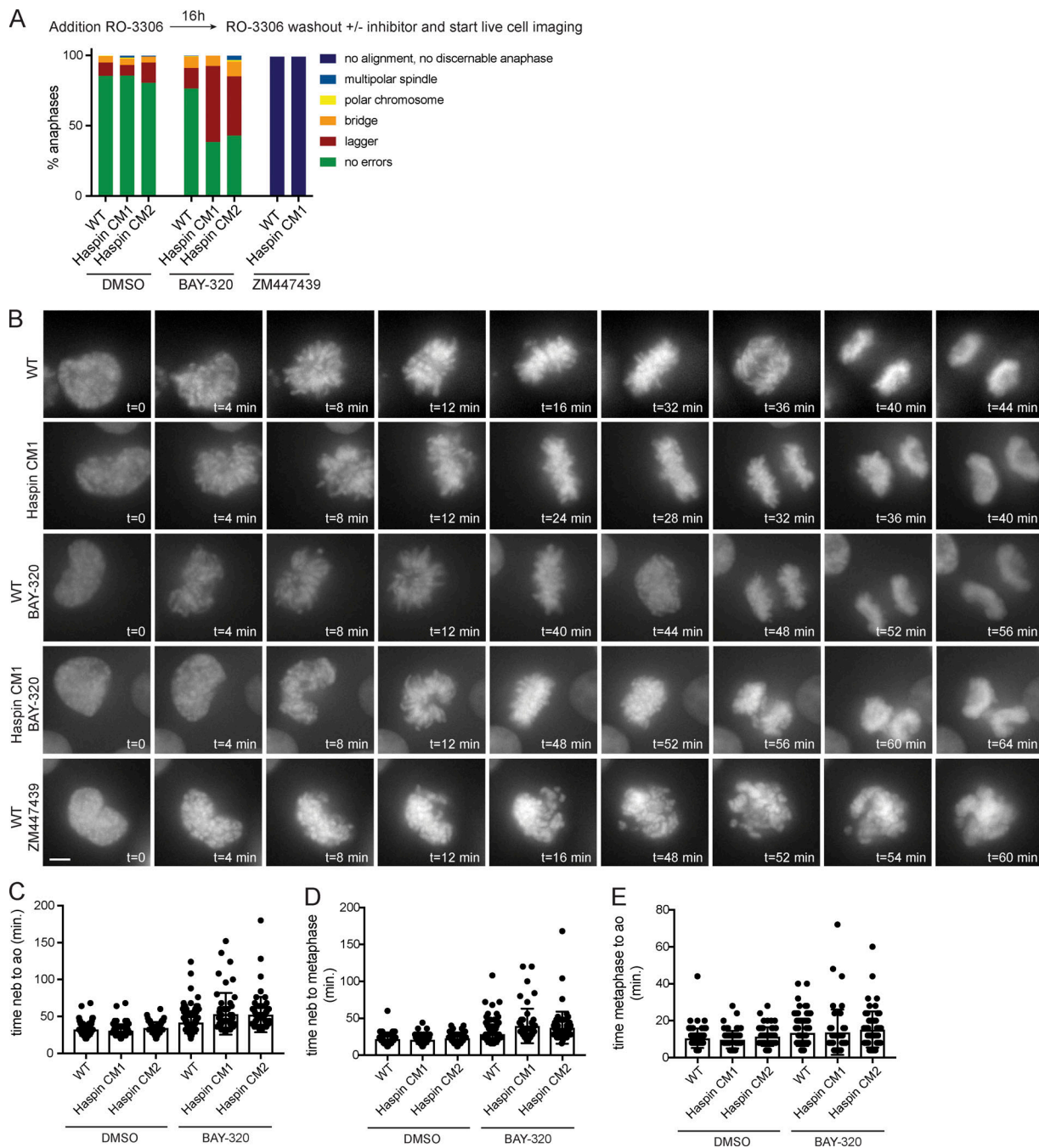
Figure 3. **Effect of Haspin inactivation and Bub1 inhibition on mitotic progression. (A)** Quantification of anaphase categories (%) of H2B-mCherry expressing HCT116 WT or Haspin CM cells ±10 µM BAY-320, as determined by live cell imaging. The experimental setup is schematically depicted on top. Data are compiled from at least two independent experiments with a minimum of 14 cells per condition in each experiment, with the exception of ZM447439-treated cells, which are from a single experiment with a minimum of 33 cells per condition. **(B)** Representative stills from the live cell imaging experiment (scale bar, 5 µm). Time (min) after nuclear envelope breakdown (t = 0) is indicated. **(C–E)** Timing of nuclear envelope breakdown (neb) to anaphase onset (ao; C), neb to metaphase (D), and metaphase to ao (E) in cells progressing through mitosis. The graphs show quantifications from individual cells (dots) and the mean (bar) ± SD.

2008). Cells were blocked in mitosis after release from a G2 arrest into nocodazole in the presence or absence of BAY-320 (Fig. 5, A–D). Remarkably, phosphorylation of both Hec1 at S44 and Dsn1 at S109 were not affected by Haspin knockout, Bub1 inhibition, or the combined loss of Haspin and Bub1 activity (Fig. 5, A–D). This is in line with the notion that loss of

centromeric Aurora B still permits residual Aurora B activity (Fig. 3).

Since the net phosphorylation status of a kinase substrate depends on the balance between kinase and phosphatase activity, we tested if perturbation of Haspin and Bub1 activity might reduce the activity of local phosphatases that counteract Dsn1
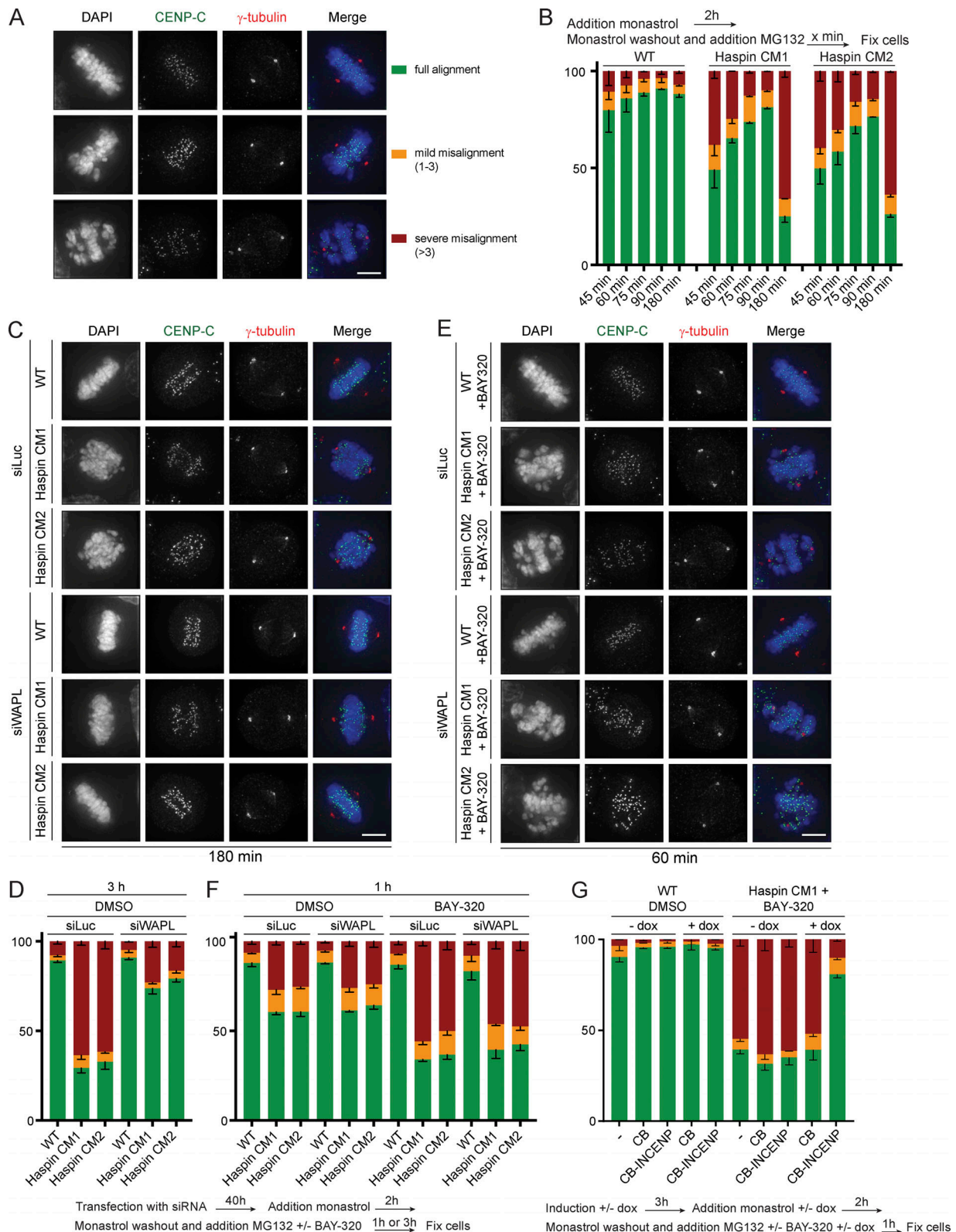
Figure 4. **Centromere relocalization of Aurora B rescues chromosome alignment in Haspin and Bub1 inhibited cells. (A)** Representative images of alignment categories observed after monastrol washout into MG132 (scale bar, 5 µm). **(B)** Quantification of chromosome alignment categories (%) following a monastrol washout into MG132 ±10 µM BAY-320 for various time points. The experimental setup is schematically depicted on top. **(C)** Representative images of cells from D. **(D)** Quantification of chromosome alignment categories (%) after a monastrol washout into MG132 (3 h) following depletion of WAPL by transfection of siRNA (siWAPL; scale bar, 5 µm). Transfection with siLuc serves as a control. The experimental setup is schematically depicted below the graph. **(E)** Representative images of F (scale bar, 5 µm). **(F)** Quantification of chromosome alignment categories (%) after a monastrol washout into MG132 (1 h) ±10

Hadders et al.
Multiple functional pools of Aurora B

Journal of Cell Biology 8 of 20
https://doi.org/10.1083/jcb.201907087

µM BAY-320 following depletion of WAPL by siWAPL. The experimental setup is schematically depicted below the graph. **(G)** Quantification of chromosome alignment categories (%) after a monastrol washout into MG132 (1 h) ±10 µM BAY-320 in cells expressing either CB-INCENP-mCherry or CB-mCherry. Plus (+) dox indicates the presence of doxycycline to induce low expression levels of either CB-INCENPdCEN-mCherry or CB-mCherry, while minus (−) dox indicates the uninduced cells. The experimental setup is schematically depicted below the graph. All graphs depict the means (bar) ± SEM of three experiments (B, D, and F) or two experiments (E).

S109 and Hec1 S44 phosphorylation. Addition of the small molecule Aurora B inhibitor ZM447439 to WT- or Bub1-inhibited Haspin CM cells (Ditchfield et al., 2003) resulted in a comparable decrease in Dsn1 and Hec1 phosphorylation, suggesting that the activity of Aurora B counteracting phosphatases is largely unaffected in the absence of Haspin and Bub1 activity (Fig. S4, A–D). In fact, when titrating ZM447439 into Bub1-inhibited Haspin CM cells, these cells lost Dsn1 S109 phosphorylation at an even lower concentration of ZM447439 than WT cells (Fig. S4 G).

We then reasoned that while the steady-state levels of Dsn1 S109 and Hec1 S44 phosphorylation remain unchanged in mitotic cells with no visible enrichment of centromeric Aurora B, perhaps the kinetics of kinetochore substrate phosphorylation was compromised: in the absence of centromere-concentrated Aurora B, cells may require more time to phosphorylate outer-KT substrates. To test this, Dsn1 S109 and Hec1 S44 phosphorylation were followed during mitotic progression by quantitative IF. We released WT or Haspin CM cells from an RO3306-induced G2 arrest in the presence or absence of BAY-320 and discriminated early phases of mitosis by nuclear envelope breakdown. Based on DAPI (chromatin morphology) and Lamin B (nuclear envelope) staining, we identified four categories of early mitotic cells (Fig. 5 E). Phosphorylation of Dsn1 S109 was already high in the category 1 cells and only slightly increased until cells reached category 3, and no clear differences could be observed between WT- and Bub1-inhibited Haspin CM cells (Fig. 5, E and F). In WT cells, phosphorylation of Hec1 S44 increased while cells progressed through mitosis, peaking in category 3 and decreasing in metaphase (category 5), in agreement with previous observations (Fig. 5, E and G; DeLuca et al., 2006, 2011; Welburn et al., 2010). We observed a similar pattern of Hec1 S44 phosphorylation in Bub1-inhibited Haspin CM cells. However, the peak of Hec1 phosphorylation appeared to shift from category 3 to category 2 cells, indicating that the kinetics of Hec1 phosphorylation might be slightly accelerated (Fig. 5, E and G). Moreover, Hec1 S44 phosphorylation levels in metaphase appeared similar in all conditions, suggesting that dephosphorylation of Hec1 S44 in metaphase is not affected by the loss of Haspin and Bub1 activity (Fig. 5, E and G).

Finally, we also tested if the observed kinetochore phosphorylation was caused by a recently described microtubule-dependent pool of the CPC (Trivedi et al., 2019). We blocked cells in mitosis in the presence of increasing concentration of nocodazole and again measured kinetochore phosphorylation using quantitative IF. However, we saw no difference in Hec1 S44 phosphorylation using a nocodazole concentration described to fully prevent microtubule formation (3.3 µM; Fig. S4, H and I).

Taken together, our data suggest that phosphorylation of the tested outer kinetochore substrates does not require centromeric accumulation of Aurora B, and that the limited error correction efficiency observed in Bub1-inhibited Haspin CM cells cannot be explained by reduced Hec1 phosphorylation.

Regulation of MCAK localization at centromeres by Haspin and Bub1 kinase activities

We next considered reductions in the levels of centromeric MCAK (mitotic centromere-associated kinesin; KIF2C) as a possible cause of the limited error correction in Haspin- and Bub1-deficient cells. MCAK is a microtubule depolymerase that controls mitotic spindle assembly and faithful chromosome segregation (Bakhoum et al., 2009a,b; Kline-Smith et al., 2004; Maney et al., 1998; Walczak et al., 2002). Recruitment of MCAK to centromeres depends on Bub1 and Aurora B kinase activities. Specifically, Bub1 phosphorylates histone H2A T120, resulting in recruitment of Sgo2 to centromeres. Sgo2 then recruits MCAK in an Aurora B kinase–dependent manner (Huang et al., 2007; Kawashima et al., 2010; Kitajima et al., 2005; Tanno et al., 2010). MCAK recruitment was shown to be strongly reduced after loss of Haspin or Haspin activity (De Antoni et al., 2012; Wang et al., 2010, 2012), and we reasoned this might explain the delayed error correction observed in the Haspin CM cells (Fig. 4, A and B). Surprisingly, quantitative IF did not reveal an obvious decrease in centromeric MCAK levels in Haspin CM cells compared with WT cells blocked in mitosis with nocodazole (Fig. 6, A and B; and Fig. S5, A and B). siRNA-mediated knockdown of Haspin or Haspin inhibition by 5-ITu resulted in a small decrease in centromeric MCAK levels in WT HCT116 cells, but not to the extent previously reported (Fig. S5, C–H; De Antoni et al., 2012; Wang et al., 2010, 2012). Instead, we observed a redistribution of MCAK from the inner to the KT proximal centromere in Haspin CM and Haspin knockdown cells. In addition, we also observed a more continuous distribution of MCAK between the two CENP-C foci (Fig. 6 A). The displacement of MCAK followed Sgo2, in line with Sgo2 being the main MCAK receptor at centromeres (Fig. 6, C and D). After inhibition of Bub1 with BAY-320 in WT and Haspin CM cells, both MCAK and Sgo2 levels were strongly reduced (Fig. 6, A–D), supporting the idea that Bub1 activity is the main driver of MCAK centromere localization via Sgo2 (Fig. 6, A–D; Baron et al., 2016; Huang et al., 2007; Kawashima et al., 2010; Kitajima et al., 2005; Tang et al., 2004; Tanno et al., 2010; Williams et al., 2017). Indeed, both LacI-Bub1 and LacI-Sgo2 could recruit MCAK to ectopic LacO arrays both in WT and in Haspin CM cells, while Sgo1 and LacI-Haspin did not (Fig. 6, E–G; and Fig. S5, F–H).

Taken together, these data suggest that Haspin is not directly involved in the recruitment of Sgo2 and MCAK toward centromeres. However, Haspin seems to promote the inner
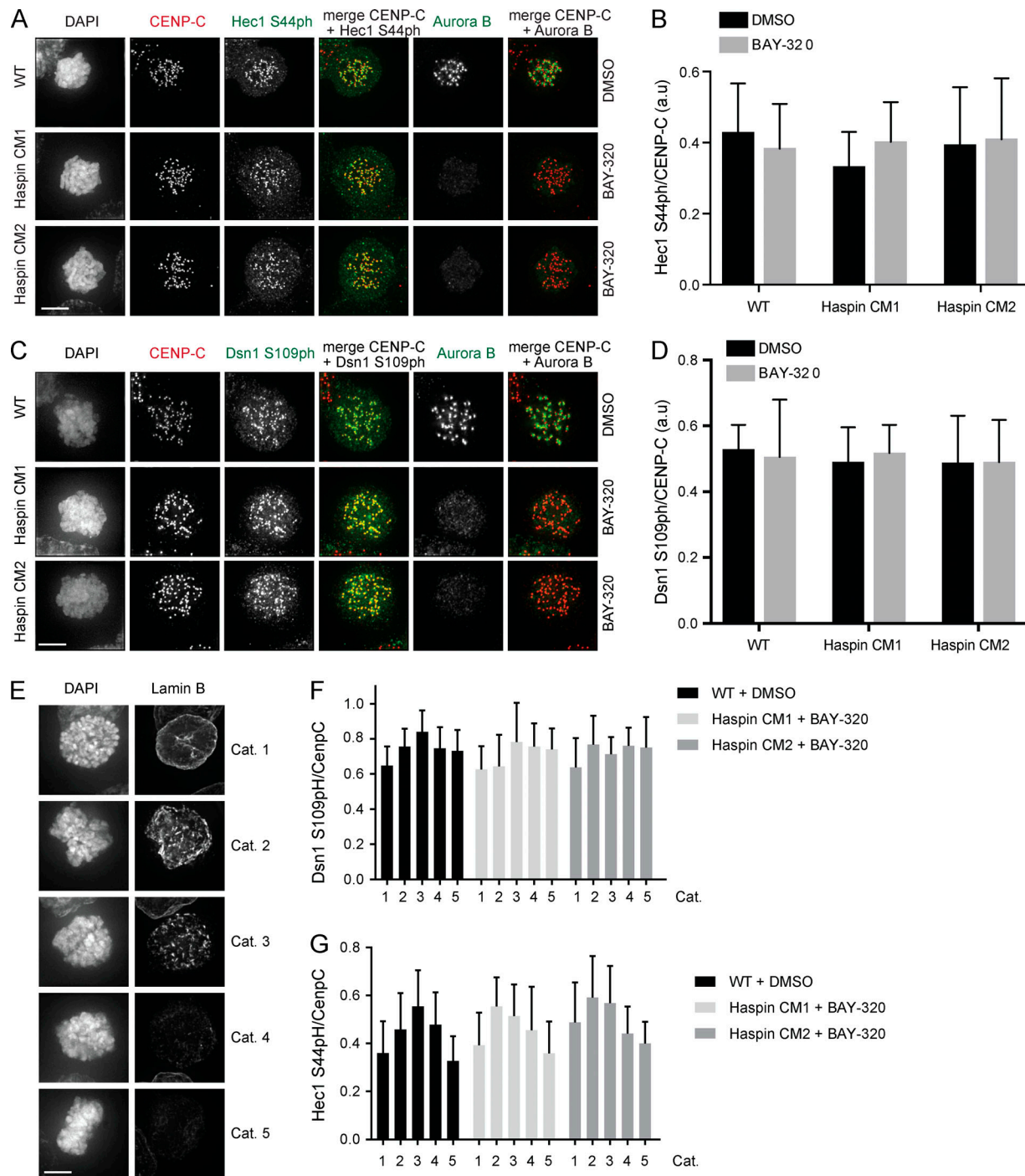
Figure 5. **Phosphorylation of the kinetochore proteins Hec1 and Dsn1 does not require centromere-concentrated Aurora B. (A–D)** IF images of Hec1 S44ph, Aurora B, and CENP-C (A) and Dsn1 S109ph, Aurora B, and CENP-C (C) of HCT116 WT and Haspin CM cells + 10 µM BAY-320, arrested in mitosis using nocodazole from a RO-3306 release (scale bar, 5 µm). **(D)** IF intensity levels of Hec1 S44ph (B) or Dsn1 S109ph (D) at kinetochores. Levels were normalized over CENP-C. The graphs show the mean and SD. A minimum of 27 cells was quantified per condition. Data are representative of two independent experiments. No significant differences were observed as determined by a two-way ANOVA using Tukey's multiple comparison test. **(E)** IF images of mitotic cells depicting DAPI and Lamin B staining. The differences in the morphology of DAPI staining and the decreasing levels of Lamin B allowed us to classify five categories of (early) mitotic cells. Cells were released from RO3036 into ±10 µM BAY-320 for 30 min (scale bar, 5 µm). For each category, we determined the IF intensity levels of Hec1 S44ph (F) or Dsn1 S109ph (G) at kinetochores in HCT116 WT and Haspin CM cells + 10 µM BAY-320.

centromere positioning of both proteins, potentially via regulation of local Aurora B activity. It remains unclear if the alternative localization of MCAK in Haspin knockout cells could explain the observed delay in chromosome alignment after monastrol wash-out (Fig. 4). The inner centromere pool of Aurora B has been suggested to inhibit the inner centromere pool of

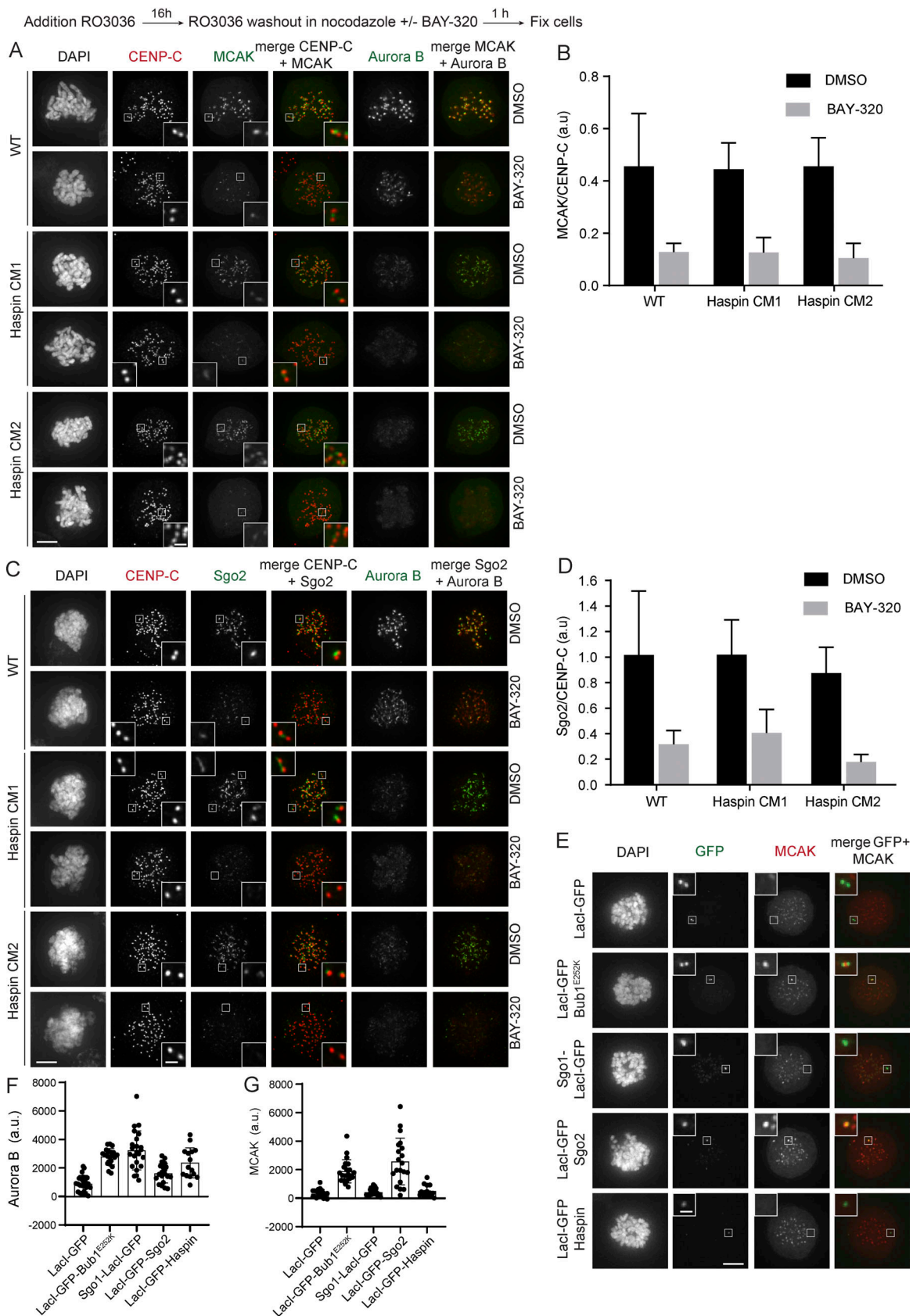Addition RO3036 —16h→ RO3036 washout in nocodazole +/- BAY-320 —1 h→ Fix cells

Figure 6. **MCAK levels are not significantly reduced in Haspin CM cells. (A–D)** IF images of MCAK, Aurora B, and CENP-C (A) and Sgo2, Aurora B, and CENP-C (C) of HCT116 WT and Haspin CM cells ±10 µM BAY-320, arrested in mitosis using nocodazole from a RO-3306 release (scale bar, 5 µm). **(B and D)** IF intensity levels of MCAK (B) or Sgo2 (D) at kinetochores. Levels were normalized over CENP-C. The graphs show the mean and SD. A minimum of 19 cells was

quantified per condition. Data are representative of two independent experiments. No significant differences were observed between WT and Haspin CM cells as determined by a two-way ANOVA using Tukey's multiple comparison test. **(E)** IF images of U-2 OS-LacO cells expressing the indicated LacI-GFP fusion proteins and arrested in prometaphase using STLC (scale bar, 5 µm). The insets show the magnification of the boxed region (scale bar, 1 µm). IF intensity levels of Aurora B (F) and MCAK (G) at the LacO-array were quantified. The graphs show quantifications from individual cells (dots) and the mean (bar) ± SD. A minimum of 15 cells was quantified per condition. Data are representative of two independent experiments.

MCAK during early mitosis, with MCAK activity rising later in mitosis when MCAK translocates toward the kinetochore, away from the inner centromere pool of Aurora B, and resolving merotelic attachments during metaphase (Andrews et al., 2004; Bakhoum et al., 2009b; Gómez et al., 2007; Knowlton et al., 2006; Lan et al., 2004; Manning et al., 2007; McHugh et al., 2019). In Haspin CM cells, Aurora B displays a similar redistribution as Sgo2 and MCAK, and may as such inhibit the activity of the alternatively localized MCAK. However, the fact that we do not observe an increase in anaphase errors in Haspin CM cells argues against this scenario (Fig. 3).

Centromere accumulation of Aurora B is dispensable for the mitotic checkpoint
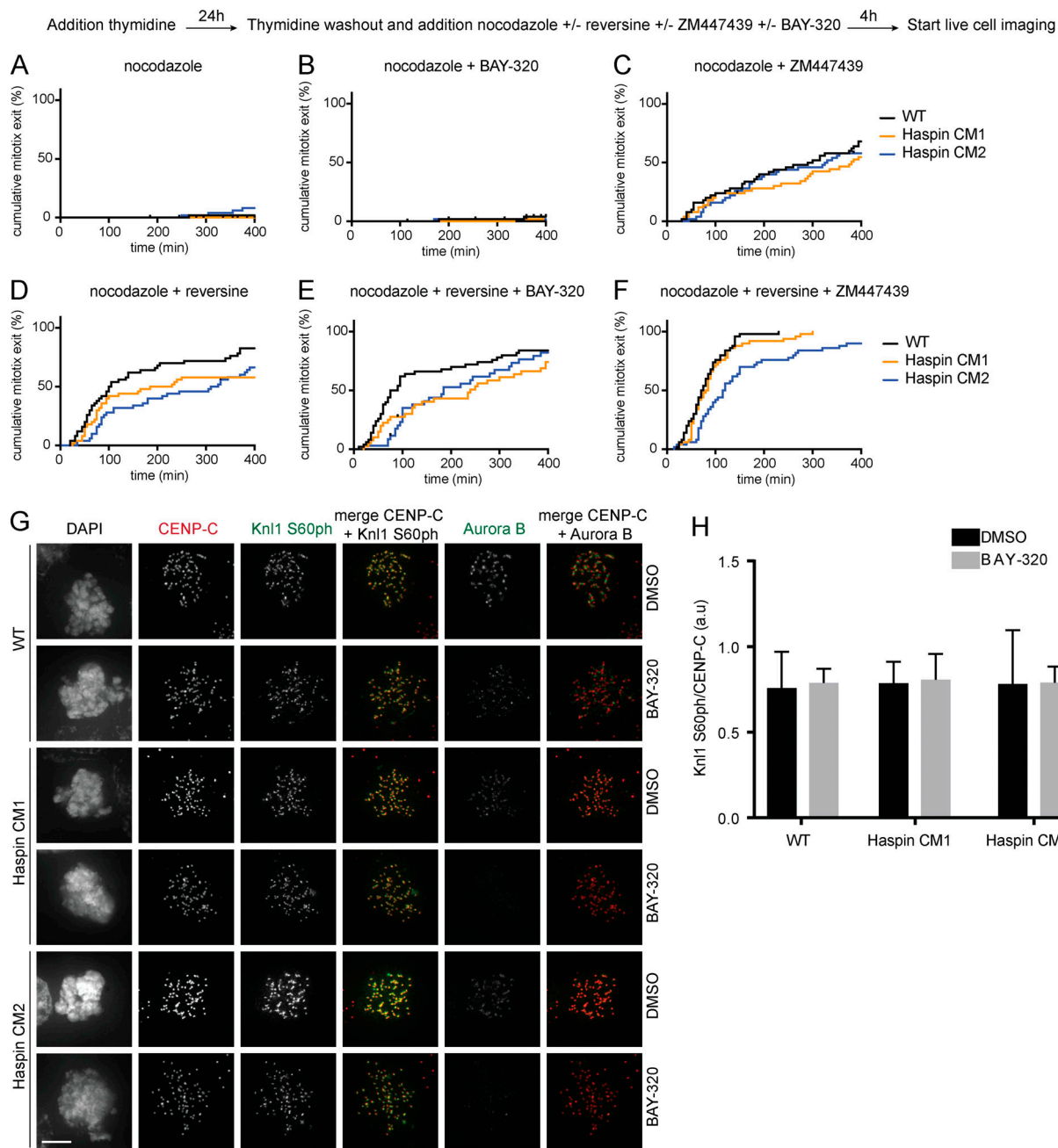
Finally, apart from regulating the stability of KT–MT attachments, Aurora B activity is also required for a robust mitotic checkpoint response (Ditchfield et al., 2003; Santaguida et al., 2011; Saurin et al., 2011; Vader et al., 2007). To examine the contribution of centromere accumulation of Aurora B in sustaining the mitotic checkpoint, we measured the time spent in mitosis in the presence of unattached kinetochores by depolymerizing spindle microtubules with a high dose of nocodazole (3.3 µM; Fig. 7). Aurora B inhibition by ZM447439 accelerated exit from mitosis in the presence of nocodazole, supporting the notion that a robust mitotic checkpoint response requires Aurora B activity (Fig. 7 C; Ditchfield et al., 2003; Santaguida et al., 2011; Saurin et al., 2011; Vader et al., 2007). However, in Bub1-inhibited Haspin CM cells, the mitotic checkpoint was strong enough to prevent mitotic exit (Fig. 7 B). To determine if Haspin CM in combination with Bub1 inhibition may have a more subtle effect on the mitotic checkpoint, we measured the extent of the mitotic delay in cells treated with nocodazole together with a low dose of reversine to partially inhibit the mitotic checkpoint kinase Mps1 (Santaguida et al., 2010). In the presence of nocodazole and reversine, WT cells gradually exited mitosis, and mitotic exit was accelerated by inhibition of Aurora B (Fig. 7, D and F), again confirming the contribution of Aurora B kinase activity to a functional mitotic checkpoint. However, even in this sensitized condition, Haspin CM, Bub1 inhibition, or a combination of these did not reduce the time spent in mitosis (Fig. 7 E), suggesting that centromeric recruitment of Aurora B by either Haspin or Bub1 is dispensable for a functional mitotic checkpoint and that the residual Aurora B kinase activity that phosphorylates the kinetochore substrates Hec1 and Dsn1 (Fig. 5) also supports a robust mitotic checkpoint response (Fig. 7). In line with this notion, we found that S60 in the RVSF motif of Knl1 is phosphorylated in nocodazole-treated Bub1-inhibited Haspin CM cells (Fig. 7, G and H). Importantly, Knl1 S60 phosphorylation was reduced to a similar extent after addition of ZM447439 in both WT and Haspin CM cells inhibited with BAY-

320, suggesting that the RVSF motif counteracting phosphatases is not perturbed by loss of Haspin and Bub1 activity (Fig. 7 H). Phosphorylation of the RVSF motif in Knl1 by Aurora B interferes with Knl1 binding to PP1γ, the phosphatase that counteracts Mps1-dependent phosphorylation of Knl1 (Liu et al., 2010; Nijenhuis et al., 2014). As such, the residual Aurora B activity may support the mitotic checkpoint.

Discussion

The combined kinase activities of Haspin and Bub1 drive the precise accumulation of Aurora B at the inner centromere and as such are thought to jointly control Aurora B activity toward kinetochore substrates involved in error correction and mitotic checkpoint activity (Hindriksen et al., 2017b; Kawashima et al., 2007, 2010; Kelly et al., 2010; Santaguida et al., 2011; Saurin et al., 2011; Tsukahara et al., 2010; Wang et al., 2010; Yamagishi et al., 2010). Here, we demonstrate that either Haspin or Bub1 kinase activity is sufficient to recruit Aurora B to an ectopic chromatin locus, and in line with this, we identified two centromere pools of Aurora B. First, inhibition of Bub1 activity revealed a Haspin-dependent pool of Aurora B that accumulated along the inter sister chromatid axis and at the inner centromere, as previously observed by others (Baron et al., 2016; Boyarchuk et al., 2007; Kawashima et al., 2007; Vanoosthuyse et al., 2007; Yamagishi et al., 2010). Second, loss of Haspin activity in Haspin CM cells exposed a small Bub1-dependent kinetochore-proximal pool of Aurora B in Haspin CM cells. This kinetochore-proximal pool of Aurora B was also infrequently observed in WT HCT116 cells, and we therefore propose that this Bub1-dependent kinetochore-proximal pool of Aurora B is present, but masked by the much higher levels of Aurora B recruited to the inner centromere by Haspin.

Recruitment of the CPC to the inner centromere is thought to serve several purposes. First, it locally concentrates and clusters the CPC, which is required to fully activate Aurora B (Kelly et al., 2007, 2010; Krenn and Musacchio, 2015; Wang et al., 2011; Zaytsev et al., 2016). Second, it is thought to confer Aurora B substrate specificity as it places the kinase in proximity to its substrates at the kinetochore (Fu et al., 2009; Hans et al., 2009; van der Horst and Lens, 2014). Third, CPC inner centromere localization would support tension-dependent phosphoregulation of Aurora B kinetochore substrates: In the presence of inter-kinetochore tension, Aurora B confined to the inner centromere is no longer be able to reach its substrates at the kinetochore, and hence only bi-oriented KT–MT attachments would be stabilized (Andrews et al., 2004; Liu et al., 2009; Tanaka et al., 2002; Welburn et al., 2010). However, we find that either the Haspin or the Bub1 kinase-dependent pools of Aurora B can largely support faithful chromosome segregation in

Addition thymidine —24h→ Thymidine washout and addition nocodazole +/- reversine +/- ZM447439 +/- BAY-320 —4h→ Start live cell imaging

Figure 7. Haspin inactivation and Bub1 inhibition do not impair the mitotic checkpoint. (A–F) Cumulative mitotic exit over time for HCT116 WT or Haspin CM cells in the presence of 3.3 µM nocodazole (A–C) or 3.3 µM nocodazole + 200 nM reversine (D–F). The effects of Aurora B inhibition (2 µM ZM447439) or Bub1 inhibition (10 µM BAY-320) on mitotic timing are shown. The experimental setup is schematically depicted above the graphs. Black dots indicate cell death. Note that the data line stops when 100% mitotic exit is reached. A minimum of 25 cells was analyzed per condition. Data are representative of at least two independent experiments per condition. **(G)** IF images of Knl1 S60ph, Aurora B, and CENP-C of HCT116 WT and Haspin CM cells + 10 µM BAY-320, arrested in mitosis using nocodazole from a RO-3306 release (scale bar, 5 µm). **(H)** IF intensity levels of Knl1 S60ph at kinetochores. Levels were normalized over CENP-C. The graphs show the mean and SD. A minimum of 19 cells was quantified per condition. Data are representative of two independent experiments. No significant differences were observed as determined by a two-way ANOVA using Tukey's multiple comparison test.

otherwise unchallenged cells. These findings challenge the spatial separation model that is based on the assumption that there is a single pool of Aurora B at the inner centromere, and kinetochore substrates are phosphorylated depending on their distance from this pool (Andrews et al., 2004; Liu et al., 2009; Tanaka et al., 2002; Welburn et al., 2010). However, our findings are in line with several recent studies concluding that the

precise inner centromere localization of Aurora B is not a prerequisite for chromosome bi-orientation. Removal of the N-terminal centromere targeting domain of INCENP in budding yeast disturbed Aurora B recruitment to centromeres, but did not affect its capacity to bi-orient KT–MT attachments (Campbell and Desai, 2013). Moreover, placing Aurora B in closer proximity to the kinetochore in mammalian cells did not

impair the stabilization of bi-oriented KT–MT attachments (Hengeveld et al., 2017).

Inhibition of Bub1 kinase activity in Haspin CM cells abolished any detectable enrichment of Aurora B at centromeres. While this impaired KT–MT error correction, it did not alter the phosphorylation of the Aurora B kinetochore substrates Dsn1, Hec1, and Knl1, nor did it weaken the mitotic checkpoint. This implies that Aurora B–dependent kinetochore substrate phosphorylation and mitotic checkpoint function do not necessarily require (inner) centromere accumulation of Aurora B. Because activation of Aurora B depends on clustering of the CPC (Kelly et al., 2007, 2010; Wang et al., 2011), clustering and activation of Aurora B most likely takes place at an alternative location, in the absence of Haspin and Bub1 activity. This could simply be chromatin, as we observed low levels of Aurora B dispersed over the chromatin in Bub1-inhibited Haspin CM cells, and in *Xenopus laevis* egg extracts this was shown to be sufficient for the activation of Aurora B kinase activity (Haase et al., 2017; Kelly et al., 2007). Alternatively, recent work proposed a role for microtubules that traverse the centromere in depositing active Aurora B from the centromere at the kinetochore (Trivedi et al., 2019). A Borealin mutant incapable of binding microtubules in vitro was unable to rescue KT substrate phosphorylation, despite the presence of active Aurora B at centromeres. We deem it unlikely that a microtubule-associated pool of the CPC is responsible for the KT substrate phosphorylation in Bub1-inhibited Haspin CM cells because we observed no difference in Hec1 phosphorylation in either low (0.33 µM) or high (3.3 µM) concentrations of nocodazole. However, we cannot exclude that the CPC core complex, consisting of Borealin, Survivin, and the N terminus of INCENP, might play a role in Aurora B–dependent KT substrate phosphorylation independently of microtubule binding and inner centromere clustering of Aurora B (Haase et al., 2017). Finally, a potential third, transient kinetochore-associated pool of Aurora B, one that does not depend on Haspin and Bub1 kinase activity, may phosphorylate the KMN network (Caldas et al., 2013; DeLuca et al., 2011; Fischböck-Halwachs et al., 2019; García-Rodríguez et al., 2019; Broad et al., 2020).

Irrespective of the source of Aurora B activity that can phosphorylate substrates within the microtubule binding KMN network, in cells with combined Haspin and Bub1 inhibition, impaired error correction does not correlate with a reduction in Hec1 and Dsn1 phosphorylation. This seems to be in line with a recent study by Yoo et al. (2018), who used a fluorescence lifetime imaging microscopy–Förster resonance energy transfer–based approach to estimate the fraction of Hec1/Ndc80 complexes bound to kMTs. While inhibition of Haspin by the small molecule inhibitor 5-ITu reduced the accumulation of Aurora B at centromeres and increased kMT binding to Hec1/Ndc80 in the absence of tension, it did not reduce phosphorylation of an Aurora B Förster resonance energy transfer probe that was localized at the outer-KT (Yoo et al., 2018). This suggests that KT–MT dynamics and hence error correction efficiency are more sensitive to reductions in Aurora B centromeric levels than the phosphorylation of KMN substrates and mitotic checkpoint activity. In fact, we deem it likely that the observed phosphorylation of KMN substrates in Bub1-inhibited Haspin CM cells could explain their capacity to sustain the mitotic checkpoint in nocodazole with partial inhibition of Mps1. Phosphorylation of these outer kinetochore substrates by Aurora B, including the RVSF motif in Knl1, would prevent the recruitment of PP1γ, thereby precluding PP1γ-mediated dephosphorylation of Mps1-phosphorylated MELT motifs in Knl1, a prerequisite for mitotic checkpoint silencing (Hengeveld et al., 2017; Liu et al., 2010; London et al., 2012; Meadows et al., 2011; Nijenhuis et al., 2014; Rosenberg et al., 2011; Shepperd et al., 2012; Yamagishi et al., 2012). Of note, based on experiments using the Haspin inhibitors 5-ITu and LDN-211898, it was concluded that Haspin is important for mitotic checkpoint signaling, either directly or indirectly through localization of Aurora B (De Antoni et al., 2012; Wang et al., 2012). In contrast, we find that Haspin CM cells sustain the mitotic checkpoint in nocodazole even when the checkpoint kinase Mps1 was partially inhibited (Fig. 7, D and E). Therefore, our data argue against a role for Haspin in the mitotic checkpoint.

Our findings raise the question how the loss of the Aurora B centromere pools impairs KT–MT error correction, when Hec1 can still be phosphorylated. The Bub1-dependent pool of Aurora B in Haspin CM cells supports chromosome alignment in otherwise unchallenged cells, but is less efficient in bi-orienting chromosomes when the frequency of erroneous KT–MT attachments is increased. Further reducing centromeric levels of Aurora B by inhibition of Bub1 exacerbates the alignment defect in Haspin CM cells. One could argue the latter might be caused by a loss of the microtubule-destabilizing kinesin MCAK from centromeres, which is present at very low levels in Bub1-inhibited Haspin CM cells. However, the levels of centromeric MCAK are already very low in Bub1-inhibited WT cells that do align efficiently when released from a mitotic arrest induced by Eg5 inhibition. Moreover, the observation that expression of CB-INCENP can rescue alignment in Bub1-inhibited Haspin CM cells argues against a role for centromeric MCAK levels, but again suggests that the total level of Aurora B at centromeres is an important determinant for efficient resolution of erroneous attachments. Additionally, it shows that the bi-orientation defects observed upon loss of Haspin and Bub1 activity can be attributed to loss of centromeric Aurora B and not to loss of Aurora B–independent functions of Haspin or Bub1. The Aurora B substrates involved remain to be identified, but we expect these to be specifically phosphorylated by the centromere-associated pools of Aurora B.

In conclusion, we have uncovered at least three different functional pools of Aurora B: a Haspin-dependent inner centromere pool, a Bub1-dependent kinetochore proximal pool, and a Haspin- and Bub1-independent pool, responsible for phosphorylation of kinetochore substrates. The Haspin- and Bub1-dependent Aurora B pools are largely redundant for KT–MT error correction. We propose that through phosphorylation of proteins at the kinetochore, the third pool contributes to mitotic checkpoint signaling but also regulates KT–MT attachments.

Together, these three pools of Aurora B ensure that chromosome segregation occurs with high fidelity even in challenging conditions.

Hadders et al.
Multiple functional pools of Aurora B

Journal of Cell Biology 14 of 20
https://doi.org/10.1083/jcb.201907087

Materials and methods

Cell culture and cell lines

U-2 OS-LacO cells (Janicki et al., 2004) were cultured in DMEM (Sigma-Aldrich) supplemented with 10% FBS (Bodinco BV), 2 mM UltraGlutamine (Lonza), 100 U/ml penicillin, and 100 µg/ml streptomycin (Lonza). HCT116 cells (a kind gift from O. Kranenburg, University Medical Center Utrecht, Utrecht, Netherlands) were cultured in DMEM F12 (Lonza) supplemented with 10% FBS, 2 mM UltraGlutamine, 100 U/ml penicillin, 100 µg/ml streptomycin, and 25 mM Hepes (Lonza). Cell lines were maintained at 37°C and 5% CO_2. HCT116 cells stably expressing H2B-mCherry were generated by lentiviral transduction as described before (Hengeveld et al., 2017). Briefly, HEK293T cells (ATCC, CRL-3216) were cotransfected with pWPT-H2B-mCherry, pRSV, pMD2-G, and pMDLG-I using X-tremeGENE (Roche) according to the manufacturer's instructions. After 48 h, viruses were harvested and used for viral transduction of HCT116 cells. HCT116 cells expressing doxycycline-inducible CB-INCENPdCEN-mCherry and CB-mCherry were generated by lentiviral transduction as described above and selected on G418. Sf9 cells (ATCC, CRL-1711) were cultured in Insect-EXPRESS (Lonza) supplemented with 5% heat-inactivated FBS, 100 U/ml penicillin, and 100 µg/ml streptomycin. Cells were maintained at 27°C in suspension flasks.

Plasmids

sgRNAs targeting GSG2 are 5′-GCAATGATTTTTATGGCTAC-3′ (U-2 OS-LacO Haspin CM), 5′-CAAGTGGTGCTCCGTCCTCT-3′ (HCT116 Haspin CM1), and 5′-CGTCCGCAGCCCCATATGTG-3′ (HCT116 Haspin CM2). sgRNAs were cloned into pAceBac-Cas9 (Hindriksen et al., 2017a). Bacmids were generated using the Bac-to-Bac system in conjunction with EMBacY cells (Berger et al., 2004; Bieniossek et al., 2012).

LacI-GFP, LacI-GFP-Haspin, LacI-GFP-Haspin kinase dead (K511A), LacI-GFP-Bub1, LacI-GFP-Bub1[E252K], LacI-GFP-Bub1[E252K] kinase dead (D946A), Sgo1-LacI-GFP, or LacI-GFP-Sgo2 was cloned into pAceBac1-CMV or pAceBac1-Ubc (van der Horst et al., 2015). Bacmids were generated using the Bac-to-Bac system in conjunction with EMBacY cells (Berger et al., 2004; Bieniossek et al., 2012). For generating doxycycline-inducible HCT116 cells, CB-INCENPdCEN-mCherry and CB-mCherry were cloned into pInducer20.

Baculovirus production and transduction

Baculovirus was produced by transfection of bacmids into Sf9 cells as described previously (Hindriksen et al., 2017a). For baculoviral transduction, cells were trypsinized and taken up in DMEM F12 supplemented with 10% heat-inactivated FBS, 2 mM UltraGlutamine, 100 U/ml penicillin, and 100 µg/ml streptomycin. Cells were plated, and baculovirus was added immediately.

Generation of Haspin CM cell lines

U-2 OS LacO and HCT116 Haspin knockout cells were generated using CRISPR/Cas9. Briefly, cells were transduced with recombinant baculovirus expressing Cas9-2a-GFP and the gRNA

sequences indicated above. After 48 h, cells were seeded at low density in 96-well plates. Cells from wells harboring single colonies were selected for further analysis.

Genotyping of Haspin CM cell lines

Genomic DNA was isolated using the DNeasy Blood and Tissue kit (Qiagen), and PCR was performed using the following primers: Haspin-Fw: 5′-AAACACCTCCTCAGAGTGATCCCAGGA GATCTCTGC-3′; and Haspin-Rv: 5′-TTACTTAAACAGACTGTG CTGGCAGAGCAAGTCAGTG-3′. PCR products were subjected to Sanger sequencing.

siRNA transfection

The following siRNAs were used in this study: Luciferase (siLuc, 20 or 100 nM, Luciferase GL2 duplex; Dharmacon/D-001 100–01-20), Bub1 (siBub1, 100 nM, 5′-GAAUGUAAGCGUU-CACGAADTDT-3′; Dharmacon), WAPL (siWAPL, 40 nM, 5′-GAGAGAUGUUUACGAGUUUDTDT-3′; Dharmacon), and Haspin (siGSG2, 40 nM, Ambion AM51331, ID1093). Cells were plated and transfected immediately using HiPerfect (Qiagen) or DharmaFECT 2 (Dharmacon), according to the manufacturers' instructions.

IF microscopy

Cells were cultured on 12-mm glass coverslips and synchronized in mitosis by the addition of either S-trityl-L-cysteine (STLC; Tocris Bioscience; 20 µM) or nocodazole (Sigma-Aldrich; 0.83 µM), as indicated in the figure legends. Alternatively, cells were blocked in G2 by using the CDK1 inhibitor RO-3036 (Calbiochem; 7.5 µM) overnight. The next morning, RO-3036 was washed away in the presence of nocodazole (0.83 µM), leaving the cells another 1–4 h in the presence or absence of BAY-320 (10 µM), ZM447493 (2 µM), 5-ITu (2 µM), or DMSO as a control. For the LMNB1 experiments, the cells were released after overnight RO-3306 block for 30 min.

Cells were fixed using PFA, permeabilizing cells either before or after fixation. In the first case, cells were treated with 0.2% Triton X-100 (vol/vol) in PEM buffer (100 mM Pipes KOH, pH 6.8, 5 mM EGTA, and 1 mM $MgCl_2$) for ±60 s. Next, an equal volume of 4% PFA in PBS was added (final concentration, 2% PFA). 4 min later, this was replaced with 4% PFA in PBS and incubated for another 4 min. For IF staining of Hec1 S44ph, Knl1 S60pH and Dsn1 S109pH cells were first permeabilized in 0.25% Saponin (wt/vol) in PHEM buffer (60 mM Pipes, 20 mM Hepes KOH, pH 6.9, 10 mM EGTA, and 4 mM $MgSO_4$) for ±3 min, followed by fixation of cells in 4% PFA in PHEM buffer for ±10 min. For the permeabilization after fixation, cells were treated with 0.5% Triton X-100 in PBS for 1 min. For Histon3 T3ph, Histon2A T120pH and MCAK cells were fixed with 4% PFA in PBS for 10 min. After two washes with PBS, the cells were incubated in ice-cold methanol for a minimum of 20 min. Cells were washed with PBS and then blocked with 3% BSA in PBS with 0.01% Tween 20 (PBST0.01).

Cells were incubated with primary antibodies diluted in 3% BSA in PBST0.01 for 2 h. After washing with PBST0.01, cells were incubated with secondary antibodies with or without GFP-Booster (Chromotek, cat. no. ABIN509419, 1:5,000) diluted in 3%

Hadders et al.
Multiple functional pools of Aurora B

Journal of Cell Biology
https://doi.org/10.1083/jcb.201907087

15 of 20

BSA in PBST0.01 for 1 h. After washing with PBST0.01, cells were treated with 500 ng/ml DAPI in PBST0.01 for a few minutes. After a final wash in PBS, the coverslips were mounted onto glass slides using Prolong Diamond Antifade Mountant (Thermo Fisher Scientific).

Images were acquired on a DeltaVision imaging system (GE Healthcare), upgraded with a seven-color InsightSSI Module & TruLight Illumination System Module using a UPlanSApo 100×/1.40 objective and a CoolSnap HQ2 camera (Photometrics). Presented images are deconvolved maximum intensity projections, processed using Softworx v6. Quantifications were performed using an in-house-developed macro in ImageJ that automatically selects kinetochores. This selection was enlarged with 3 pixels (px), and this region of interest (ROI) was then used to measure fluorescence intensities in different channels. For the Knl1 S60ph and Hec1 S44ph, the ROI of the centrosomes staining was removed for the images. For background subtraction, an area surrounding the DAPI signal was selected. This area was enlarged with 4 px (ROI-A) and with 6 px (ROI-B). ROI-A was subtracted from ROI-B, and this selected region was used to determine the background fluorescence.

Primary antibodies used were anti-Aurora B (Millipore, cat. no. EP1009Y, rabbit monoclonal, 1:1,000), anti-Aurora B (BD Transductions, cat. no. 611083, mouse monoclonal, 1:500), anti-CENP-C (MBL International, cat. no. PD030, guinea pig polyclonal, 1:1,000), anti-CENP-T (MBL International, cat. no. D286-3, rat monoclonal, 1:500, discontinued) anti-phospho-Histone H3 (Thr3; Merck Millipore, cat. no. 07–424, rabbit polyclonal, 1:2,000), anti-phospho-Histone H3 (Thr3; Southern Biotech, cat no. 13500–01, mouse monoclonal, 1:4,000–1:8,000), anti-Sgo1 (Abnova, cat. no. h00151648, mouse monoclonal, 1:1,000), anti-Sgo2 (Novus, cat. no. NB100-60454, rabbit polyclonal, 1:1,000), anti-MCAK (Abcam, cat. no. ab187652, rabbit polyclonal, 1:500), anti-H2AT120ph (Active Motif, cat. no. 39391, rabbit polyclonal, 1:2,000), anti-LMNB1 (Atlas antibodies, cat. no AMAB-91251, monoclonal, 1:1,000), and anti-Dsn1 (GeneTex, GTX120402, rabbit polyclonal, 1:1,000). Anti-Knl1 (rabbit, polyclonal, 1:500) was a kind gift from G. Kops, Hubrecht Institute–KNAW, University Medical Center Utrecht, Utrecht, Netherlands. Anti-phospho-Dsn1 (S109; rabbit polyclonal, 1:1,000) and phosphor-Knl1 (S60; rabbit polyclonal, 1:2,000) were kind gifts from I. Cheeseman, Whitehead Institute for Biomedical Research, Massachusetts Institute of Technology, Cambridge, MA (Welburn et al., 2010). Anti-phospho-Hec1 (S44; rabbit polyclonal, 1:2,000) was a kind gift from J. DeLuca, Colorado State University, Fort Collins, CO (DeLuca et al., 2011).

Secondary antibodies used were goat anti-mouse IgG Alexa Fluor 488 conjugate (Thermo Fisher Scientific, cat. no. A-11029, 1:500), goat anti-mouse IgG Alexa Fluor 568 conjugate (Thermo Fisher Scientific, cat. no. A-11031, 1:500), goat anti-mouse IgG Alexa Fluor 647 conjugate (Thermo Fisher Scientific, cat. no. A-1103121236, 1:500), goat anti-rabbit IgG Alexa Fluor 488 conjugate (Thermo Fisher Scientific, cat. no. A-11034, 1:500), goat anti-rabbit IgG Alexa Fluor 568 conjugate (Thermo Fisher Scientific, cat. no. A-11036, 1:500), goat anti-rabbit IgG Alexa Fluor 647 conjugate (Thermo Fisher Scientific, cat. no. A-21245,

1:500), and goat anti-guinea pig IgG Alexa Fluor 647 conjugate (Thermo Fisher Scientific, cat. no. A-21450, 1:500).

Chromosome alignment assay
To assay chromosome alignment, cells were incubated with 5 µM monastrol for ±2 h. Cells were then washed three times with medium, after which medium containing 5 µM MG-132 (Merck Millipore) with or without 10 µM BAY-320 was added for various times (45–180 min) before fixing the cells as described above. For the inducible HCT116 cells, induction with 1 µg/ml doxycycline was started 6 h before fixing the cells.

Chromosome spreads
For the preparation of chromosome spreads, HCT116 cells were treated with 0.83 µM nocodazole for 3 h before harvesting by mitotic shake off. Cells were then incubated in 75 mM KCl for 10 min (room temperature) and spun onto coverslips for 4 min at 800 rpm using a Shandon Cytospin 4 (Thermo Fisher Scientific). Cells were then fixed and stained as described above. CENP-C/CENP-C distances were calculated using the x, y, and z coordinates of the centroids of CENP-C kinetochore pairs, obtained from 3D z-stacks using the 3D objects counter in FIJI. Line plots were generated with the Plot Profile tool in FIJI.

Western blotting
Cells were synchronized for 6 h with 0.83 µM nocodazole and harvested. Protein concentrations were determined using a Lowry assay to ensure equal sample loading. Proteins were separated by SDS-PAGE using a Bolt 4–12% Bis-Tris Plus gel (Thermo Fisher Scientific, cat. no. NW0412BOX). Proteins were then transferred to nitrocellulose membranes using a Trans-Blot Turbo Transfer system (Bio-Rad, cat. no. 170–4155). Membranes were blocked in PBST containing 3% BSA. Primary antibody incubation was performed in PBST including 3% BSA for ~18 h at 4°C. Membranes were washed three times with PBST before incubation with the secondary antibody diluted in PBST. Membranes were washed three more times followed by signal detection using ECL.

Primary antibodies used were anti-Aurora B (ARK-2; Santa Cruz, sc-25426, rabbit polyclonal, 1:1,000), anti-phospho-Histone H3 (Thr3; Southern Biotech, 13500-01, mouse monoclonal, 1:1,000), and anti-α-tubulin (Sigma-Aldrich, cat. no. T5168, mouse monoclonal, 1:10,000). Secondary antibodies used were swine anti-rabbit-HRP (DAKO, P0217, 1:2,500) and rabbit anti-mouse-HRP (DAKO, P0161, 1:2,500).

Live cell imaging
Cells were seeded in eight-well imaging chambers (µ-Slide, Ibidi) and blocked in G2 by overnight incubation in 7.5 µM RO-3306. The cells were released from the RO-3306 block by washing three times with warm medium, followed directly by filming. Film experiments were performed on a DeltaVision imaging system with an imaging chamber maintained at 37°C and 5% CO$_2$ (GE Healthcare). The system was upgraded with a seven-color InsightSSI Module and TruLight Illumination System Module and made use of an Olympus UApo N340 40×/1.35 objective and a CoolSnap HQ2 camera (Photometrics).

Hadders et al.
Multiple functional pools of Aurora B

Journal of Cell Biology 16 of 20
https://doi.org/10.1083/jcb.201907087

For assessing the duration of the mitotic arrest in nocodazole by live cell imaging, cells were first seeded in eight-well imaging chambers (µ-Slide, Ibidi) and treated with 2.5 mM thymidine (Sigma-Aldrich) for 24 h. Cells were washed three times with medium, after which culture medium was changed to Leibovitz's L-15 medium (Gibco), supplemented with 10% FBS, 2 mM UltraGlutamine (Lonza), 100 U/ml penicillin, and 100 µg/ml streptomycin (Lonza), containing 3.3 µM nocodazole. ZM447439 (2 µM; Tocris Bioscience), reversine (200 nM; Cayman Chemical), and/or BAY-320 (10 µM; gift from Bayer Pharma AG; Baron et al., 2016) were added as indicated. Cells were imaged on an Olympus Cell M system with a UPlanFL N 20×/0.5 objective and analyzed using ImageJ software.

Online supplemental material

Fig. S1 shows the quantified levels of GFP for the various LacI-GFP fusions expressed in Figs. 1 and 2 (A–H and Q), shows recruitment of Aurora B by both Sgo1-LacI-GFP and LacI-GFP-Sgo2 (I–K), shows Aurora B recruitment by LacI-GFP-Haspin upon depletion of Bub1 (L–O), and shows a Western blot showing loss of H3T3 phosphorylation in U-2 OS LacO Haspin CM cells (P). Fig. S2 shows IF images and quantifications highlighting loss of H3T3 phosphorylation in HCT116 Haspin CM cell lines (A–C), shows a Western blot depicting loss of H3T3 phosphorylation in HCT116 Haspin CM cell lines (D), and shows a quantification of an IF experiment determining centromeric Sgo1 levels in the presence or absence of BAY-320 in HCT116 WT and Haspin CM cells (E). Fig. S3 shows a quantification of a chromosome alignment assay of HCT116 WT and Haspin CM cells with or without Bub1 inhibition upon depletion of WAPL (A) and shows IF images and quantifications of HCT116 WT and Haspin CM cells expressing CB-INCENP, which rescues centromeric levels of Aurora B (B and C). Fig. S4 shows IF images and quantifications of HCT116 WT and Haspin CM for Dsn1 S109, Hec1 S44, and Knl1 S60 phosphorylation with or without Aurora B inhibition (A–F), shows IF quantification of Dsn1 S109 phosphorylation at various concentrations of ZM447439 in HCT116 WT and Haspin CM cells (G), and shows IF quantification of Hec1 S44 phosphorylation and tubulin in HCT116 WT and Haspin CM cells at various concentrations of nocodazole (H–I). Fig. S5 shows IF images and quantifications of HCT116 cells with or without depletion of MCAK using two different siRNAs to validate our MCAK antibody (A and B), shows IF images and quantifications of MCAK levels in HCT116 cells with depletion (C–E) or inhibition (F–H) of Haspin (activity), and shows IF images and quantifications of U-2 OS LacO WT and Haspin CM cells expressing various LacI-GFP fusion proteins and their ability to recruit MCAK (I–K). Table S1 summarizes the alterations induced by Cas9 at the GSG2 locus in the cell lines used in this study, both at the genetic level and the resultant protein level.

Acknowledgments

We thank Dr. I. Cheeseman and Dr. G. Kops for their generous gift of antibodies and Dr. G. Siemeister from Bayer AG, Berlin, Germany, for the generous gift of BAY-320.

References

Andrews, P.D., Y. Ovechkina, N. Morrice, M. Wagenbach, K. Duncan, L. Wordeman, and J.R. Swedlow. 2004. Aurora B regulates MCAK at the mitotic centromere. *Dev. Cell.* 6:253–268. https://doi.org/10.1016/S1534-5807(04)00025-5

Bakhoum, S.F., G. Genovese, and D.A. Compton. 2009a. Deviant kinetochore microtubule dynamics underlie chromosomal instability. *Curr. Biol.* 19:1937–1942. https://doi.org/10.1016/j.cub.2009.09.055

Bakhoum, S.F., S.L. Thompson, A.L. Manning, and D.A. Compton. 2009b. Genome stability is ensured by temporal control of kinetochore-microtubule dynamics. *Nat. Cell Biol.* 11:27–35. https://doi.org/10.1038/ncb1809

Baron, A.P., C. von Schubert, F. Cubizolles, G. Siemeister, M. Hitchcock, A. Mengel, J. Schröder, A. Fernández-Montalván, F. von Nussbaum, D. Mumberg, and E.A. Nigg. 2016. Probing the catalytic functions of Bub1 kinase using the small molecule inhibitors BAY-320 and BAY-524. *eLife.* 5:e12187. https://doi.org/10.7554/eLife.12187

Bekier, M.E., T. Mazur, M.S. Rashid, and W.R. Taylor. 2015. Borealin dimerization mediates optimal CPC checkpoint function by enhancing localization to centromeres and kinetochores. *Nat. Commun.* 6:6775. https://doi.org/10.1038/ncomms7775

Berger, I., D.J. Fitzgerald, and T.J. Richmond. 2004. Baculovirus expression system for heterologous multiprotein complexes. *Nat. Biotechnol.* 22:1583–1587. https://doi.org/10.1038/nbt1036

Bieniossek, C., T. Imasaki, Y. Takagi, and I. Berger. 2012. MultiBac: expanding the research toolbox for multiprotein complexes. *Trends Biochem. Sci.* 37:49–57. https://doi.org/10.1016/j.tibs.2011.10.005

Boyarchuk, Y., A. Salic, M. Dasso, and A. Arnaoutov. 2007. Bub1 is essential for assembly of the functional inner centromere. *J. Cell Biol.* 176:919–928. https://doi.org/10.1083/jcb.200609044

Broad, A.J., K.F. DeLuca, and J.G. DeLuca. 2020. Aurora B kinase is recruited to multiple discrete kinetochore and centromere regions in human cells. *J. Cell Biol.* https://doi.org/10.1083/jcb.201905144

Caldas, G.V., K.F. DeLuca, and J.G. DeLuca. 2013. KNL1 facilitates phosphorylation of outer kinetochore proteins by promoting Aurora B kinase activity. *J. Cell Biol.* 203:957–969. https://doi.org/10.1083/jcb.201306054

Campbell, C.S., and A. Desai. 2013. Tension sensing by Aurora B kinase is independent of survivin-based centromere localization. *Nature.* 497:118–121. https://doi.org/10.1038/nature12057

Cheeseman, I.M., J.S. Chappie, E.M. Wilson-Kubalek, and A. Desai. 2006. The conserved KMN network constitutes the core microtubule-binding site of the kinetochore. *Cell.* 127:983–997. https://doi.org/10.1016/j.cell.2006.09.039

Cimini, D., X. Wan, C.B. Hirel, and E.D. Salmon. 2006. Aurora kinase promotes turnover of kinetochore microtubules to reduce chromosome segregation errors. *Curr. Biol.* 16:1711–1718. https://doi.org/10.1016/j.cub.2006.07.022

Dai, J., S. Sultan, S.S. Taylor, and J.M. Higgins. 2005. The kinase haspin is required for mitotic histone H3 Thr 3 phosphorylation and normal metaphase chromosome alignment. *Genes Dev.* 19:472–488. https://doi.org/10.1101/gad.1267105

Dai, J., B.A. Sullivan, and J.M. Higgins. 2006. Regulation of mitotic chromosome cohesion by Haspin and Aurora B. *Dev. Cell.* 11:741–750. https://doi.org/10.1016/j.devcel.2006.09.018

Hadders et al.
Multiple functional pools of Aurora B

Journal of Cell Biology 17 of 20
https://doi.org/10.1083/jcb.201907087

Dai, J., A.V. Kateneva, and J.M. Higgins. 2009. Studies of haspin-depleted cells reveal that spindle-pole integrity in mitosis requires chromosome cohesion. *J. Cell Sci.* 122:4168–4176. https://doi.org/10.1242/jcs.054122

De Antoni, A., S. Maffini, S. Knapp, A. Musacchio, and S. Santaguida. 2012. A small-molecule inhibitor of Haspin alters the kinetochore functions of Aurora B. *J. Cell Biol.* 199:269–284. https://doi.org/10.1083/jcb.201205119

DeLuca, J.G., W.E. Gall, C. Ciferri, D. Cimini, A. Musacchio, and E.D. Salmon. 2006. Kinetochore microtubule dynamics and attachment stability are regulated by Hec1. *Cell.* 127:969–982. https://doi.org/10.1016/j.cell.2006.09.047

DeLuca, K.F., S.M. Lens, and J.G. DeLuca. 2011. Temporal changes in Hec1 phosphorylation control kinetochore-microtubule attachment stability during mitosis. *J. Cell Sci.* 124:622–634. https://doi.org/10.1242/jcs.072629

Ditchfield, C., V.L. Johnson, A. Tighe, R. Ellston, C. Haworth, T. Johnson, A. Mortlock, N. Keen, and S.S. Taylor. 2003. Aurora B couples chromosome alignment with anaphase by targeting BubR1, Mad2, and Cenp-E to kinetochores. *J. Cell Biol.* 161:267–280. https://doi.org/10.1083/jcb.200208091

Du, J., A.E. Kelly, H. Funabiki, and D.J. Patel. 2012. Structural basis for recognition of H3T3ph and Smac/DIABLO N-terminal peptides by human Survivin. *Structure.* 20:185–195. https://doi.org/10.1016/j.str.2011.12.001

Fischböck-Halwachs, J., S. Singh, M. Potocnjak, G. Hagemann, V. Solis-Mezarino, S. Woike, M. Ghodgaonkar-Steger, F. Weissmann, L.D. Gallego, J. Rojas, et al. 2019. The COMA complex interacts with Cse4 and positions Sli15/Ipl1 at the budding yeast inner kinetochore. *eLife.* 8:e42879. https://doi.org/10.7554/eLife.42879

Foley, E.A., and T.M. Kapoor. 2013. Microtubule attachment and spindle assembly checkpoint signalling at the kinetochore. *Nat. Rev. Mol. Cell Biol.* 14:25–37. https://doi.org/10.1038/nrm3494

Fu, J., M. Bian, J. Liu, Q. Jiang, and C. Zhang. 2009. A single amino acid change converts Aurora-A into Aurora-B-like kinase in terms of partner specificity and cellular function. *Proc. Natl. Acad. Sci. USA.* 106:6939–6944. https://doi.org/10.1073/pnas.0900833106

Ganem, N.J., S.A. Godinho, and D. Pellman. 2009. A mechanism linking extra centrosomes to chromosomal instability. *Nature.* 460:278–282. https://doi.org/10.1038/nature08136

García-Rodríguez, L.J., T. Kasciukovic, V. Denninger, and T.U. Tanaka. 2019. Aurora B-INCENP Localization at Centromeres/Inner Kinetochores Is Required for Chromosome Bi-orientation in Budding Yeast. *Curr. Biol.* 29:1536–1544. https://doi.org/10.1016/j.cub.2019.03.051

Girdler, F., F. Sessa, S. Patercoli, F. Villa, A. Musacchio, and S. Taylor. 2008. Molecular basis of drug resistance in aurora kinases. *Chem. Biol.* 15:552–562. https://doi.org/10.1016/j.chembiol.2008.04.013

Gómez, R., A. Valdeolmillos, M.T. Parra, A. Viera, C. Carreiro, F. Roncal, J.S. Rufas, J.L. Barbero, and J.A. Suja. 2007. Mammalian SGO2 appears at the inner centromere domain and redistributes depending on tension across centromeres during meiosis II and mitosis. *EMBO Rep.* 8:173–180. https://doi.org/10.1038/sj.embor.7400877

Haase, J., M.K. Bonner, H. Halas, and A.E. Kelly. 2017. Distinct Roles of the Chromosomal Passenger Complex in the Detection of and Response to Errors in Kinetochore-Microtubule Attachment. *Dev. Cell.* 42:640–654.e5. https://doi.org/10.1016/j.devcel.2017.08.022

Hans, F., D.A. Skoufias, S. Dimitrov, and R.L. Margolis. 2009. Molecular distinctions between Aurora A and B: a single residue change transforms Aurora A into correctly localized and functional Aurora B. *Mol. Biol. Cell.* 20:3491–3502. https://doi.org/10.1091/mbc.e09-05-0370

Harrington, E.A., D. Bebbington, J. Moore, R.K. Rasmussen, A.O. Ajose-Adeogun, T. Nakayama, J.A. Graham, C. Demur, T. Hercend, A. Diu-Hercend, et al. 2004. VX-680, a potent and selective small-molecule inhibitor of the Aurora kinases, suppresses tumor growth in vivo. *Nat. Med.* 10:262–267. https://doi.org/10.1038/nm1003

Hauf, S., R.W. Cole, S. LaTerra, C. Zimmer, G. Schnapp, R. Walter, A. Heckel, J. van Meel, C.L. Rieder, and J.M. Peters. 2003. The small molecule Hesperadin reveals a role for Aurora B in correcting kinetochore-microtubule attachment and in maintaining the spindle assembly checkpoint. *J. Cell Biol.* 161:281–294. https://doi.org/10.1083/jcb.200208092

Hengeveld, R.C.C., M.J.M. Vromans, M. Vleugel, M.A. Hadders, and S.M.A. Lens. 2017. Inner centromere localization of the CPC maintains centromere cohesion and allows mitotic checkpoint silencing. *Nat. Commun.* 8:15542. https://doi.org/10.1038/ncomms15542

Hindriksen, S., A.J. Bramer, M.A. Truong, M.J.M. Vromans, J.B. Post, I. Verlaan-Klink, H.J. Snippert, S.M.A. Lens, and M.A. Hadders. 2017a. Baculoviral delivery of CRISPR/Cas9 facilitates efficient genome editing in human cells. *PLoS One.* 12:e0179514. https://doi.org/10.1371/journal.pone.0179514

Hindriksen, S., S.M.A. Lens, and M.A. Hadders. 2017b. The Ins and Outs of Aurora B Inner Centromere Localization. *Front. Cell Dev. Biol.* 5:112. https://doi.org/10.3389/fcell.2017.00112

Huang, H., J. Feng, J. Famulski, J.B. Rattner, S.T. Liu, G.D. Kao, R. Muschel, G.K. Chan, and T.J. Yen. 2007. Tripin/hSgo2 recruits MCAK to the inner centromere to correct defective kinetochore attachments. *J. Cell Biol.* 177:413–424. https://doi.org/10.1083/jcb.200701122

Huang, H., M. Lampson, A. Efimov, and T.J. Yen. 2018. Chromosome instability in tumor cells due to defects in Aurora B mediated error correction at kinetochores. *Cell Cycle.* 17:2622–2636. https://doi.org/10.1080/15384101.2018.1553340

Janicki, S.M., T. Tsukamoto, S.E. Salghetti, W.P. Tansey, R. Sachidanandam, K.V. Prasanth, T. Ried, Y. Shav-Tal, E. Bertrand, R.H. Singer, and D.L. Spector. 2004. From silencing to gene expression: real-time analysis in single cells. *Cell.* 116:683–698. https://doi.org/10.1016/S0092-8674(04)00171-0

Jeyaprakash, A.A., C. Basquin, U. Jayachandran, and E. Conti. 2011. Structural basis for the recognition of phosphorylated histone h3 by the survivin subunit of the chromosomal passenger complex. *Structure.* 19:1625–1634. https://doi.org/10.1016/j.str.2011.09.002

Kapoor, T.M., T.U. Mayer, M.L. Coughlin, and T.J. Mitchison. 2000. Probing spindle assembly mechanisms with monastrol, a small molecule inhibitor of the mitotic kinesin, Eg5. *J. Cell Biol.* 150:975–988. https://doi.org/10.1083/jcb.150.5.975

Kawashima, S.A., T. Tsukahara, M. Langegger, S. Hauf, T.S. Kitajima, and Y. Watanabe. 2007. Shugoshin enables tension-generating attachment of kinetochores by loading Aurora to centromeres. *Genes Dev.* 21:420–435. https://doi.org/10.1101/gad.1497307

Kawashima, S.A., Y. Yamagishi, T. Honda, K. Ishiguro, and Y. Watanabe. 2010. Phosphorylation of H2A by Bub1 prevents chromosomal instability through localizing shugoshin. *Science.* 327:172–177. https://doi.org/10.1126/science.1180189

Kelly, A.E., S.C. Sampath, T.A. Maniar, E.M. Woo, B.T. Chait, and H. Funabiki. 2007. Chromosomal enrichment and activation of the aurora B pathway are coupled to spatially regulate spindle assembly. *Dev. Cell.* 12:31–43. https://doi.org/10.1016/j.devcel.2006.11.001

Kelly, A.E., C. Ghenoiu, J.Z. Xue, C. Zierhut, H. Kimura, and H. Funabiki. 2010. Survivin reads phosphorylated histone H3 threonine 3 to activate the mitotic kinase Aurora B. *Science.* 330:235–239. https://doi.org/10.1126/science.1189505

Khodjakov, A., L. Copenagle, M.B. Gordon, D.A. Compton, and T.M. Kapoor. 2003. Minus-end capture of preformed kinetochore fibers contributes to spindle morphogenesis. *J. Cell Biol.* 160:671–683. https://doi.org/10.1083/jcb.200208143

Kim, S., and H. Yu. 2015. Multiple assembly mechanisms anchor the KMN spindle checkpoint platform at human mitotic kinetochores. *J. Cell Biol.* 208:181–196. https://doi.org/10.1083/jcb.201407074

Kitajima, T.S., S. Hauf, M. Ohsugi, T. Yamamoto, and Y. Watanabe. 2005. Human Bub1 defines the persistent cohesion site along the mitotic chromosome by affecting Shugoshin localization. *Curr. Biol.* 15:353–359. https://doi.org/10.1016/j.cub.2004.12.044

Kline-Smith, S.L., A. Khodjakov, P. Hergert, and C.E. Walczak. 2004. Depletion of centromeric MCAK leads to chromosome congression and segregation defects due to improper kinetochore attachments. *Mol. Biol. Cell.* 15:1146–1159. https://doi.org/10.1091/mbc.e03-08-0581

Knowlton, A.L., W. Lan, and P.T. Stukenberg. 2006. Aurora B is enriched at merotelic attachment sites, where it regulates MCAK. *Curr. Biol.* 16:1705–1710. https://doi.org/10.1016/j.cub.2006.07.057

Krenn, V., and A. Musacchio. 2015. The Aurora B Kinase in Chromosome Bi-Orientation and Spindle Checkpoint Signaling. *Front. Oncol.* 5:225. https://doi.org/10.3389/fonc.2015.00225

Krenn, V., A. Wehenkel, X. Li, S. Santaguida, and A. Musacchio. 2012. Structural analysis reveals features of the spindle checkpoint kinase Bub1-kinetochore subunit Knl1 interaction. *J. Cell Biol.* 196:451–467. https://doi.org/10.1083/jcb.201110013

Lampson, M.A., and I.M. Cheeseman. 2011. Sensing centromere tension: Aurora B and the regulation of kinetochore function. *Trends Cell Biol.* 21:133–140. https://doi.org/10.1016/j.tcb.2010.10.007

Lampson, M.A., K. Renduchitala, A. Khodjakov, and T.M. Kapoor. 2004. Correcting improper chromosome-spindle attachments during cell division. *Nat. Cell Biol.* 6:232–237. https://doi.org/10.1038/ncb1102

Lan, W., X. Zhang, S.L. Kline-Smith, S.E. Rosasco, G.A. Barrett-Wilt, J. Shabanowitz, D.F. Hunt, C.E. Walczak, and P.T. Stukenberg. 2004. Aurora B

phosphorylates centromeric MCAK and regulates its localization and microtubule depolymerization activity. *Curr. Biol.* 14:273–286. https://doi.org/10.1016/j.cub.2004.01.055

Larsen, N.A., J. Al-Bassam, R.R. Wei, and S.C. Harrison. 2007. Structural analysis of Bub3 interactions in the mitotic spindle checkpoint. *Proc. Natl. Acad. Sci. USA.* 104:1201–1206. https://doi.org/10.1073/pnas.0610358104

Liang, C., Q. Chen, Q. Yi, M. Zhang, H. Yan, B. Zhang, L. Zhou, Z. Zhang, F. Qi, S. Ye, and F. Wang. 2018. A kinase-dependent role for Haspin in antagonizing Wapl and protecting mitotic centromere cohesion. *EMBO Rep.* 19:43–56. https://doi.org/10.15252/embr.201744737

Liu, D., G. Vader, M.J. Vromans, M.A. Lampson, and S.M. Lens. 2009. Sensing chromosome bi-orientation by spatial separation of aurora B kinase from kinetochore substrates. *Science.* 323:1350–1353. https://doi.org/10.1126/science.1167000

Liu, D., M. Vleugel, C.B. Backer, T. Hori, T. Fukagawa, I.M. Cheeseman, and M.A. Lampson. 2010. Regulated targeting of protein phosphatase 1 to the outer kinetochore by KNL1 opposes Aurora B kinase. *J. Cell Biol.* 188:809–820. https://doi.org/10.1083/jcb.201001006

Liu, H., L. Jia, and H. Yu. 2013. Phospho-H2A and cohesin specify distinct tension-regulated Sgo1 pools at kinetochores and inner centromeres. *Curr. Biol.* 23:1927–1933. https://doi.org/10.1016/j.cub.2013.07.078

Liu, H., Q. Qu, R. Warrington, A. Rice, N. Cheng, and H. Yu. 2015. Mitotic Transcription Installs Sgo1 at Centromeres to Coordinate Chromosome Segregation. *Mol. Cell.* 59:426–436. https://doi.org/10.1016/j.molcel.2015.06.018

London, N., S. Ceto, J.A. Ranish, and S. Biggins. 2012. Phosphoregulation of Spc105 by Mps1 and PP1 regulates Bub1 localization to kinetochores. *Curr. Biol.* 22:900–906. https://doi.org/10.1016/j.cub.2012.03.052

Maney, T., A.W. Hunter, M. Wagenbach, and L. Wordeman. 1998. Mitotic centromere-associated kinesin is important for anaphase chromosome segregation. *J. Cell Biol.* 142:787–801. https://doi.org/10.1083/jcb.142.3.787

Manning, A.L., N.J. Ganem, S.F. Bakhoum, M. Wagenbach, L. Wordeman, and D.A. Compton. 2007. The kinesin-13 proteins Kif2a, Kif2b, and Kif2c/MCAK have distinct roles during mitosis in human cells. *Mol. Biol. Cell.* 18:2970–2979. https://doi.org/10.1091/mbc.e07-02-0110

Mayer, T.U., T.M. Kapoor, S.J. Haggarty, R.W. King, S.L. Schreiber, and T.J. Mitchison. 1999. Small molecule inhibitor of mitotic spindle bipolarity identified in a phenotype-based screen. *Science.* 286:971–974. https://doi.org/10.1126/science.286.5441.971

McHugh, T., J. Zou, V.A. Volkov, A. Bertin, S.K. Talapatra, J. Rappsilber, M. Dogterom, and J.P.I. Welburn. 2019. The depolymerase activity of MCAK shows a graded response to Aurora B kinase phosphorylation through allosteric regulation. *J. Cell Sci.* 132:jcs228353. https://doi.org/10.1242/jcs.228353

Meadows, J.C., L.A. Shepperd, V. Vanoosthuyse, T.C. Lancaster, A.M. Sochaj, G.J. Buttrick, K.G. Hardwick, and J.B. Millar. 2011. Spindle checkpoint silencing requires association of PP1 to both Spc7 and kinesin-8 motors. *Dev. Cell.* 20:739–750. https://doi.org/10.1016/j.devcel.2011.05.008

Meraldi, P., and P.K. Sorger. 2005. A dual role for Bub1 in the spindle checkpoint and chromosome congression. *EMBO J.* 24:1621–1633. https://doi.org/10.1038/sj.emboj.7600641

Musacchio, A., and A. Desai. 2017. A Molecular View of Kinetochore Assembly and Function. *Biology (Basel).* 6:6.

Niedzialkowska, E., F. Wang, P.J. Porebski, W. Minor, J.M. Higgins, and P.T. Stukenberg. 2012. Molecular basis for phosphospecific recognition of histone H3 tails by Survivin paralogues at inner centromeres. *Mol. Biol. Cell.* 23:1457–1466. https://doi.org/10.1091/mbc.e11-11-0904

Nijenhuis, W., G. Vallardi, A. Teixeira, G.J. Kops, and A.T. Saurin. 2014. Negative feedback at kinetochores underlies a responsive spindle checkpoint signal. *Nat. Cell Biol.* 16:1257–1264. https://doi.org/10.1038/ncb3065

Overlack, K., I. Primorac, M. Vleugel, V. Krenn, S. Maffini, I. Hoffmann, G.J. Kops, and A. Musacchio. 2015. A molecular basis for the differential roles of Bub1 and BubR1 in the spindle assembly checkpoint. *eLife.* 4: e05269. https://doi.org/10.7554/eLife.05269

Primorac, I., J.R. Weir, E. Chiroli, F. Gross, I. Hoffmann, S. van Gerwen, A. Ciliberto, and A. Musacchio. 2013. Bub3 reads phosphorylated MELT repeats to promote spindle assembly checkpoint signaling. *eLife.* 2: e01030. https://doi.org/10.7554/eLife.01030

Raaijmakers, J.A., R.G.H.P. van Heesbeen, V.A. Blomen, L.M.E. Janssen, F. van Diemen, T.R. Brummelkamp, and R.H. Medema. 2018. BUB1 Is Essential for the Viability of Human Cells in which the Spindle Assembly Checkpoint Is Compromised. *Cell Reports.* 22:1424–1438. https://doi.org/10.1016/j.celrep.2018.01.034

Ricke, R.M., K.B. Jeganathan, L. Malureanu, A.M. Harrison, and J.M. van Deursen. 2012. Bub1 kinase activity drives error correction and mitotic checkpoint control but not tumor suppression. *J. Cell Biol.* 199:931–949. https://doi.org/10.1083/jcb.201205115

Rodriguez-Rodriguez, J.A., C. Lewis, K.L. McKinley, V. Sikirzhytski, J. Corona, J. Maciejowski, A. Khodjakov, I.M. Cheeseman, and P.V. Jallepalli. 2018. Distinct Roles of RZZ and Bub1-KNL1 in Mitotic Checkpoint Signaling and Kinetochore Expansion. *Curr. Biol.* 28:3422–3429.e5. https://doi.org/10.1016/j.cub.2018.10.006

Rosenberg, J.S., F.R. Cross, and H. Funabiki. 2011. KNL1/Spc105 recruits PP1 to silence the spindle assembly checkpoint. *Curr. Biol.* 21:942–947. https://doi.org/10.1016/j.cub.2011.04.011

Santaguida, S., A. Tighe, A.M. D'Alise, S.S. Taylor, and A. Musacchio. 2010. Dissecting the role of MPS1 in chromosome biorientation and the spindle checkpoint through the small molecule inhibitor reversine. *J. Cell Biol.* 190:73–87. https://doi.org/10.1083/jcb.201001036

Santaguida, S., C. Vernieri, F. Villa, A. Ciliberto, and A. Musacchio. 2011. Evidence that Aurora B is implicated in spindle checkpoint signalling independently of error correction. *EMBO J.* 30:1508–1519. https://doi.org/10.1038/emboj.2011.70

Saurin, A.T., M.S. van der Waal, R.H. Medema, S.M. Lens, and G.J. Kops. 2011. Aurora B potentiates Mps1 activation to ensure rapid checkpoint establishment at the onset of mitosis. *Nat. Commun.* 2:316. https://doi.org/10.1038/ncomms1319

Shepperd, L.A., J.C. Meadows, A.M. Sochaj, T.C. Lancaster, J. Zou, G.J. Buttrick, J. Rappsilber, K.G. Hardwick, and J.B. Millar. 2012. Phosphodependent recruitment of Bub1 and Bub3 to Spc7/KNL1 by Mph1 kinase maintains the spindle checkpoint. *Curr. Biol.* 22:891–899. https://doi.org/10.1016/j.cub.2012.03.051

Tanaka, T.U., N. Rachidi, C. Janke, G. Pereira, M. Galova, E. Schiebel, M.J. Stark, and K. Nasmyth. 2002. Evidence that the Ipl1-Sli15 (Aurora kinase-INCENP) complex promotes chromosome bi-orientation by altering kinetochore-spindle pole connections. *Cell.* 108:317–329. https://doi.org/10.1016/S0092-8674(02)00633-5

Tang, Z., Y. Sun, S.E. Harley, H. Zou, and H. Yu. 2004. Human Bub1 protects centromeric sister-chromatid cohesion through Shugoshin during mitosis. *Proc. Natl. Acad. Sci. USA.* 101:18012–18017. https://doi.org/10.1073/pnas.0408600102

Tanno, Y., T.S. Kitajima, T. Honda, Y. Ando, K. Ishiguro, and Y. Watanabe. 2010. Phosphorylation of mammalian Sgo2 by Aurora B recruits PP2A and MCAK to centromeres. *Genes Dev.* 24:2169–2179. https://doi.org/10.1101/gad.1945310

Tao, Y., P. Zhang, F. Girdler, V. Frascogna, M. Castedo, J. Bourhis, G. Kroemer, and E. Deutsch. 2008. Enhancement of radiation response in p53-deficient cancer cells by the Aurora-B kinase inhibitor AZD1152. *Oncogene.* 27:3244–3255. https://doi.org/10.1038/sj.onc.1210990

Taylor, S.S., E. Ha, and F. McKeon. 1998. The human homologue of Bub3 is required for kinetochore localization of Bub1 and a Mad3/Bub1-related protein kinase. *J. Cell Biol.* 142:1–11. https://doi.org/10.1083/jcb.142.1.1

Trivedi, P., and P.T. Stukenberg. 2016. A Centromere-Signaling Network Underlies the Coordination among Mitotic Events. *Trends Biochem. Sci.* 41:160–174. https://doi.org/10.1016/j.tibs.2015.11.002

Trivedi, P., A.V. Zaytsev, M. Godzi, F.I. Ataullakhanov, E.L. Grishchuk, and P.T. Stukenberg. 2019. The binding of Borealin to microtubules underlies a tension independent kinetochore-microtubule error correction pathway. *Nat. Commun.* 10:682. https://doi.org/10.1038/s41467-019-08418-4

Tsukahara, T., Y. Tanno, and Y. Watanabe. 2010. Phosphorylation of the CPC by Cdk1 promotes chromosome bi-orientation. *Nature.* 467:719–723. https://doi.org/10.1038/nature09390

Vader, G., C.W. Cruijsen, T. van Harn, M.J. Vromans, R.H. Medema, and S.M. Lens. 2007. The chromosomal passenger complex controls spindle checkpoint function independent from its role in correcting microtubule kinetochore interactions. *Mol. Biol. Cell.* 18:4553–4564. https://doi.org/10.1091/mbc.e07-04-0328

van der Horst, A., and S.M. Lens. 2014. Cell division: control of the chromosomal passenger complex in time and space. *Chromosoma.* 123:25–42. https://doi.org/10.1007/s00412-013-0437-6

van der Horst, A., M.J. Vromans, K. Bouwman, M.S. van der Waal, M.A. Hadders, and S.M. Lens. 2015. Inter-domain Cooperation in INCENP Promotes Aurora B Relocation from Centromeres to Microtubules. *Cell Reports.* 12:380–387. https://doi.org/10.1016/j.celrep.2015.06.038

van der Waal, M.S., A.T. Saurin, M.J. Vromans, M. Vleugel, C. Wurzenberger, D.W. Gerlich, R.H. Medema, G.J. Kops, and S.M. Lens. 2012. Mps1

promotes rapid centromere accumulation of Aurora B. *EMBO Rep.* 13: 847–854. https://doi.org/10.1038/embor.2012.93

Vanoosthuyse, V., S. Prykhozhij, and K.G. Hardwick. 2007. Shugoshin 2 regulates localization of the chromosomal passenger proteins in fission yeast mitosis. *Mol. Biol. Cell.* 18:1657–1669. https://doi.org/10.1091/mbc.e06-10-0890

Walczak, C.E., E.C. Gan, A. Desai, T.J. Mitchison, and S.L. Kline-Smith. 2002. The microtubule-destabilizing kinesin XKCM1 is required for chromosome positioning during spindle assembly. *Curr. Biol.* 12:1885–1889. https://doi.org/10.1016/S0960-9822(02)01227-7

Wang, F., J. Dai, J.R. Daum, E. Niedzialkowska, B. Banerjee, P.T. Stukenberg, G.J. Gorbsky, and J.M. Higgins. 2010. Histone H3 Thr-3 phosphorylation by Haspin positions Aurora B at centromeres in mitosis. *Science.* 330: 231–235. https://doi.org/10.1126/science.1189435

Wang, E., E.R. Ballister, and M.A. Lampson. 2011. Aurora B dynamics at centromeres create a diffusion-based phosphorylation gradient. *J. Cell Biol.* 194:539–549. https://doi.org/10.1083/jcb.201103044

Wang, F., N.P. Ulyanova, J.R. Daum, D. Patnaik, A.V. Kateneva, G.J. Gorbsky, and J.M. Higgins. 2012. Haspin inhibitors reveal centromeric functions of Aurora B in chromosome segregation. *J. Cell Biol.* 199:251–268. https://doi.org/10.1083/jcb.201205106

Welburn, J.P., M. Vleugel, D. Liu, J.R. Yates III, M.A. Lampson, T. Fukagawa, and I.M. Cheeseman. 2010. Aurora B phosphorylates spatially distinct targets to differentially regulate the kinetochore-microtubule interface. *Mol. Cell.* 38:383–392. https://doi.org/10.1016/j.molcel.2010.02.034

Williams, S.J., A. Abrieu, and A. Losada. 2017. Bub1 targeting to centromeres is sufficient for Sgo1 recruitment in the absence of kinetochores. *Chromosoma.* 126:279–286. https://doi.org/10.1007/s00412-016-0592-7

Yamagishi, Y., T. Honda, Y. Tanno, and Y. Watanabe. 2010. Two histone marks establish the inner centromere and chromosome bi-orientation. *Science.* 330:239–243. https://doi.org/10.1126/science.1194498

Yamagishi, Y., C.H. Yang, Y. Tanno, and Y. Watanabe. 2012. MPS1/Mph1 phosphorylates the kinetochore protein KNL1/Spc7 to recruit SAC components. *Nat. Cell Biol.* 14:746–752. https://doi.org/10.1038/ncb2515

Yang, Y., F. Wu, T. Ward, F. Yan, Q. Wu, Z. Wang, T. McGlothen, W. Peng, T. You, M. Sun, et al. 2008. Phosphorylation of HsMis13 by Aurora B kinase is essential for assembly of functional kinetochore. *J. Biol. Chem.* 283:26726–26736. https://doi.org/10.1074/jbc.M804207200

Yoo, T.Y., J.M. Choi, W. Conway, C.H. Yu, R.V. Pappu, and D.J. Needleman. 2018. Measuring NDC80 binding reveals the molecular basis of tension-dependent kinetochore-microtubule attachments. *eLife.* 7:e36392. https://doi.org/10.7554/eLife.36392

Zaytsev, A.V., D. Segura-Peña, M. Godzi, A. Calderon, E.R. Ballister, R. Stamatov, A.M. Mayo, L. Peterson, B.E. Black, F.I. Ataullakhanov, et al. 2016. Bistability of a coupled Aurora B kinase-phosphatase system in cell division. *eLife.* 5:e10644. https://doi.org/10.7554/eLife.10644

Zhang, G., T. Kruse, C. Guasch Boldú, D.H. Garvanska, F. Coscia, M. Mann, M. Barisic, and J. Nilsson. 2019. Efficient mitotic checkpoint signaling depends on integrated activities of Bub1 and the RZZ complex. *EMBO J.* 38:e100977. https://doi.org/10.15252/embj.2018100977

Zhou, L., C. Liang, Q. Chen, Z. Zhang, B. Zhang, H. Yan, F. Qi, M. Zhang, Q. Yi, Y. Guan, et al. 2017. The N-Terminal Non-Kinase-Domain-Mediated Binding of Haspin to Pds5B Protects Centromeric Cohesion in Mitosis. *Curr. Biol.* 27:992–1004. https://doi.org/10.1016/j.cub.2017.02.019

Supplemental material
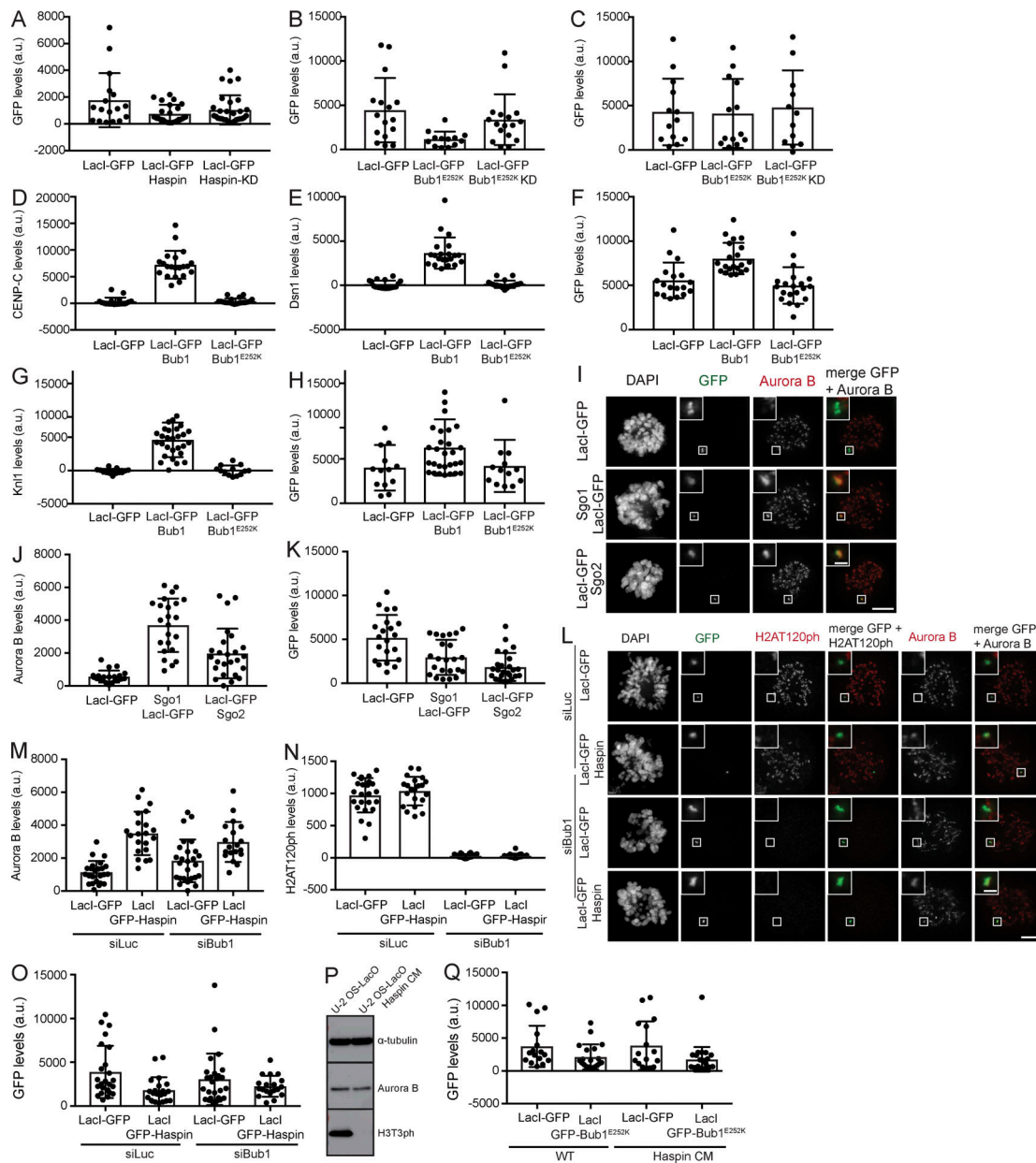
Figure S1. IF intensity levels of LacI-GFP fusion proteins at the LacO-array in U-2 OS-LacO cells. (A) IF intensity levels of GFP at the LacO-array in U-2 OS-LacO cells expressing LacI-GFP, LacI-GFP-Haspin, or LacI-GFP-Haspin kinase dead and arrested in mitosis using STLC. Corresponds with Fig. 1, C–E. The graph shows quantifications from individual cells (dots) and the mean (bar) ± SD. **(B and C)** IF intensity levels of GFP at the LacO-array in U-2 OS-LacO cells expressing LacI-GFP, LacI-GFP-Bub1^{E252K}, or LacI-GFP-Bub1^{E252K} kinase dead and arrested in mitosis using STLC. Corresponds with Fig. 1, F–K. **(B)** Corresponds to cells stained for H2AT120ph and Sgo1 (Fig. 1, F–H). **(C)** Corresponds to cells stained for Sgo2 and Aurora B (Fig. 1, I–K). The graphs show quantifications from individual cells (dots) and the mean (bar) ± SD. **(D–F)** IF intensity levels of CENP-C (A), Dsn1 (B), and GFP (C) at the LacO-array in U-2 OS-LacO cells expressing LacI-GFP, LacI-GFP-Bub1, or LacI-GFP-Bub1^{E252K} and arrested in mitosis using STLC. The graph shows quantifications from individual cells (dots) and the mean (bar) ± SD. A minimum of 18 cells was quantified per condition. **(G and H)** IF intensity levels of KNL1 (D) and GFP (E) at the LacO-array in U-2 OS-LacO cells expressing LacI-GFP, LacI-GFP-Bub1, or LacI-GFP-Bub1^{E252K} and arrested in mitosis using STLC. The graph shows quantifications from individual cells (dots) and the mean ± SD. A minimum of 13 cells was quantified per condition. **(I)** IF images of U-2 OS-LacO cells expressing the indicated Sgo LacI-GFP fusion proteins and arrested in prometaphase using STLC (scale bar, 5 μm). The insets show the magnification of the boxed region (scale bar, 1 μm). **(J and K)** IF intensity levels of Aurora B (J) or GFP (K) at the LacO-array in U-2 OS-LacO cells expressing LacI-GFP, Sgo1-LacI-GFP, or LacI-GFP-Sgo2 arrested in mitosis using STLC. The graph shows quantifications from individual cells (dots) and the mean (bar) ± SD. A minimum of 21 cells was quantified per condition. Data are representative of two independent experiments. **(L)** IF images of U-2 OS-LacO cells transfected with siLuciferase or siBub1 and expressing LacI-GFP or LacI-GFP-Haspin (scale bar, 5 μm). **(M–O)** IF intensity levels of Aurora B (M) and GFP (N) at the LacO-array, and of H2AT120ph at centromeres (O). The graphs show quantifications from individual cells (dots) and the mean (bar) ± SD. A minimum of 19 cells was quantified per condition. Data are representative of two independent experiments. **(P)** Western blot of cell lysates derived from U-2 OS-LacO and U-2 OS-LacO Haspin CM cells arrested in mitosis using nocodazole. The blot was probed for Aurora B and H3T3ph. Alpha-tubulin was used as a loading control. **(Q)** Corresponding with Fig. 1, L–N: IF intensity levels of GFP at the LacO-array in U-2 OS-LacO and U-2 OS-LacO Haspin CM cells expressing LacI-GFP or LacI-GFP-Bub1^{E252K} and arrested in mitosis using STLC. The graph shows quantifications from individual cells (dots) and the mean (bar) ± SD.
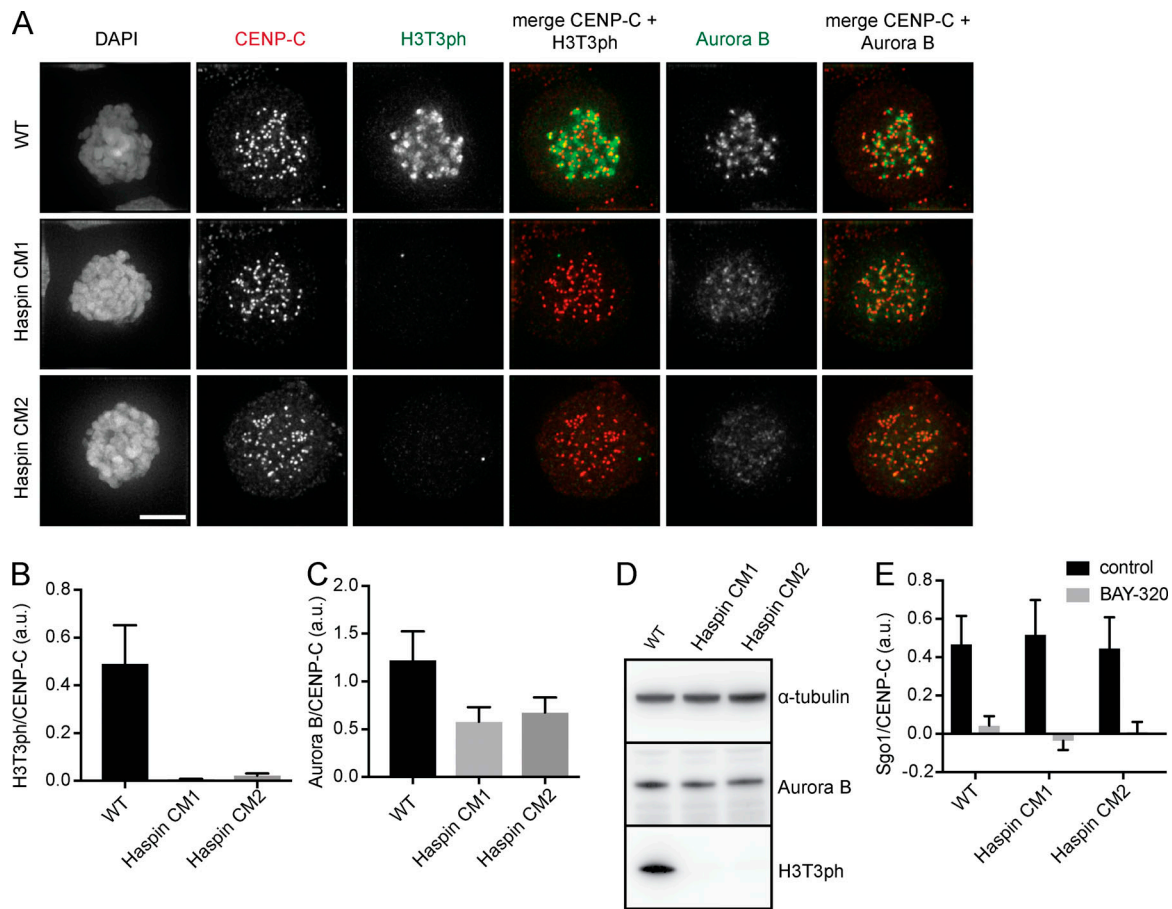
Figure S2. **Characterization of HCT116 Haspin CM cell lines and the effect of Bub1 inhibition on Sgo1 localization. (A)** IF images of HCT116 WT and Haspin CM cells arrested in mitosis using nocodazole (scale bar, 5 µm). **(B and C)** IF intensity levels of H3T3ph (B) and Aurora B (C) on centromeres. Levels were normalized over CENP-C. The graphs show the mean and SD. A minimum of 22 cells was quantified per condition. **(D)** Western blot of cell lysates derived from HCT116 WT and Haspin CM cells arrested in mitosis using nocodazole. Blot was probed for Aurora B and H3T3ph. Alpha-tubulin was used as a loading control. **(E)** IF intensity levels of Sgo1 on centromeres in HCT116 WT and Haspin CM cells ±10 µM BAY-320 arrested in mitosis using nocodazole. Levels were normalized over CENP-C. The graph shows the mean and SD. A minimum of 26 cells was quantified per condition.

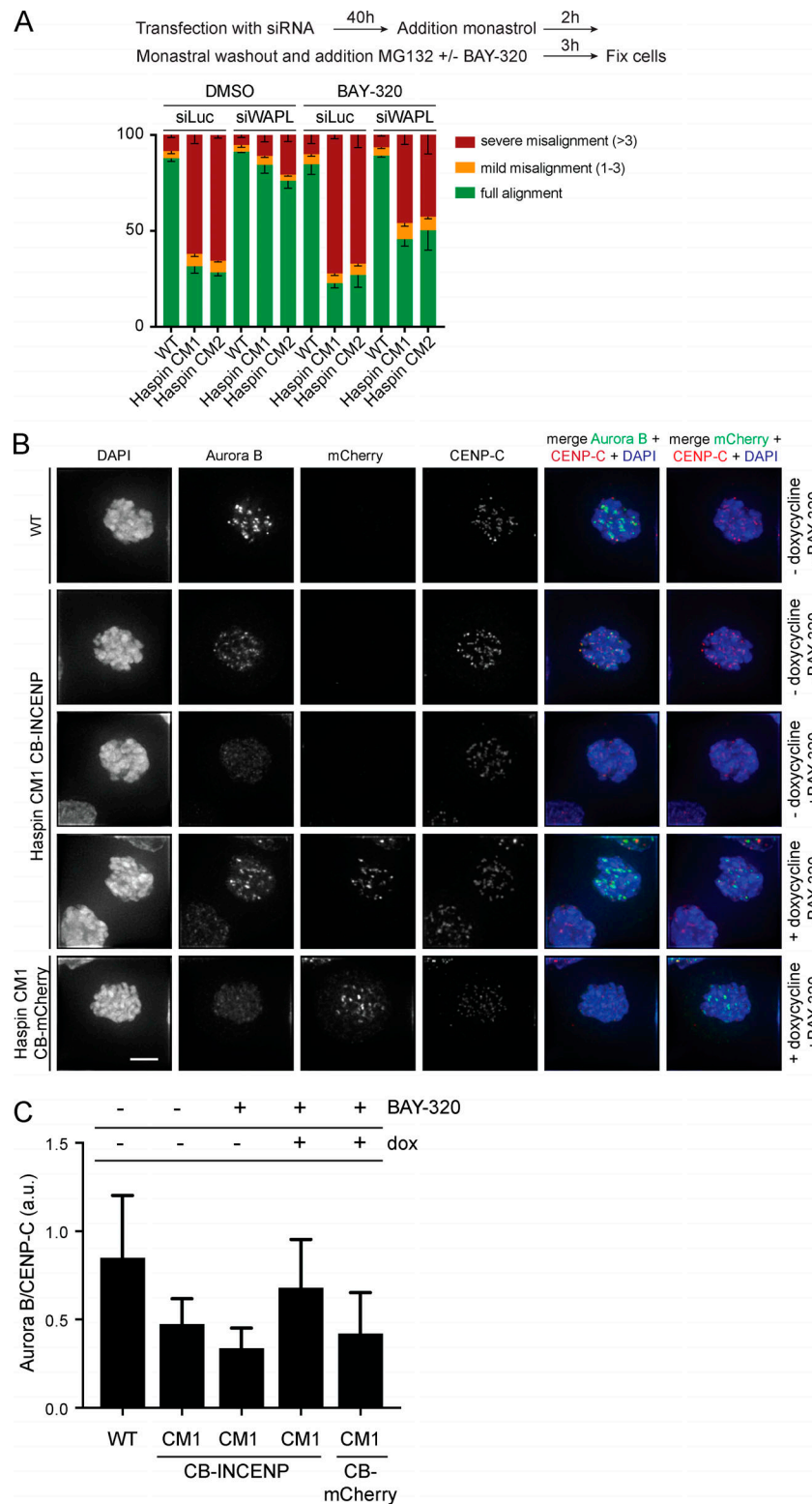**Figure S3. Effect of WAPL knockdown on chromosome alignment in Haspin- and Bub1-inhibited cells and Aurora B expression in polyclonal CB-INCENP HCT116 cell lines. (A)** Quantification of chromosome alignment categories (%) after a monastrol washout into MG132 (3 h) following depletion of WAPL by transfection of siRNA (siWAPL). Transfection with siLuc serves as a control. The experimental setup is schematically depicted on top. Graph depicts the means (bar) ± SEM of three experiments. Corresponds to Fig. 4 F. **(B)** IF images of HCT116 WT or Haspin CM cells ±10 µM BAY-320 and expressing either CB-INCENP-mCherry or CB-mCherry (scale bar, 5 µm). Plus (+) doxycycline indicates the presence of doxycycline to induce low expression levels of either CB-INCENP-mCherry or CB-mCherry. Cells were arrested in mitosis using nocodazole. **(C)** IF intensity levels of Aurora B on centromeres. Levels were normalized over CENP-C. The graphs show the mean and SD. A minimum of 19 cells was quantified per condition. Corresponds to Fig. 4 G.
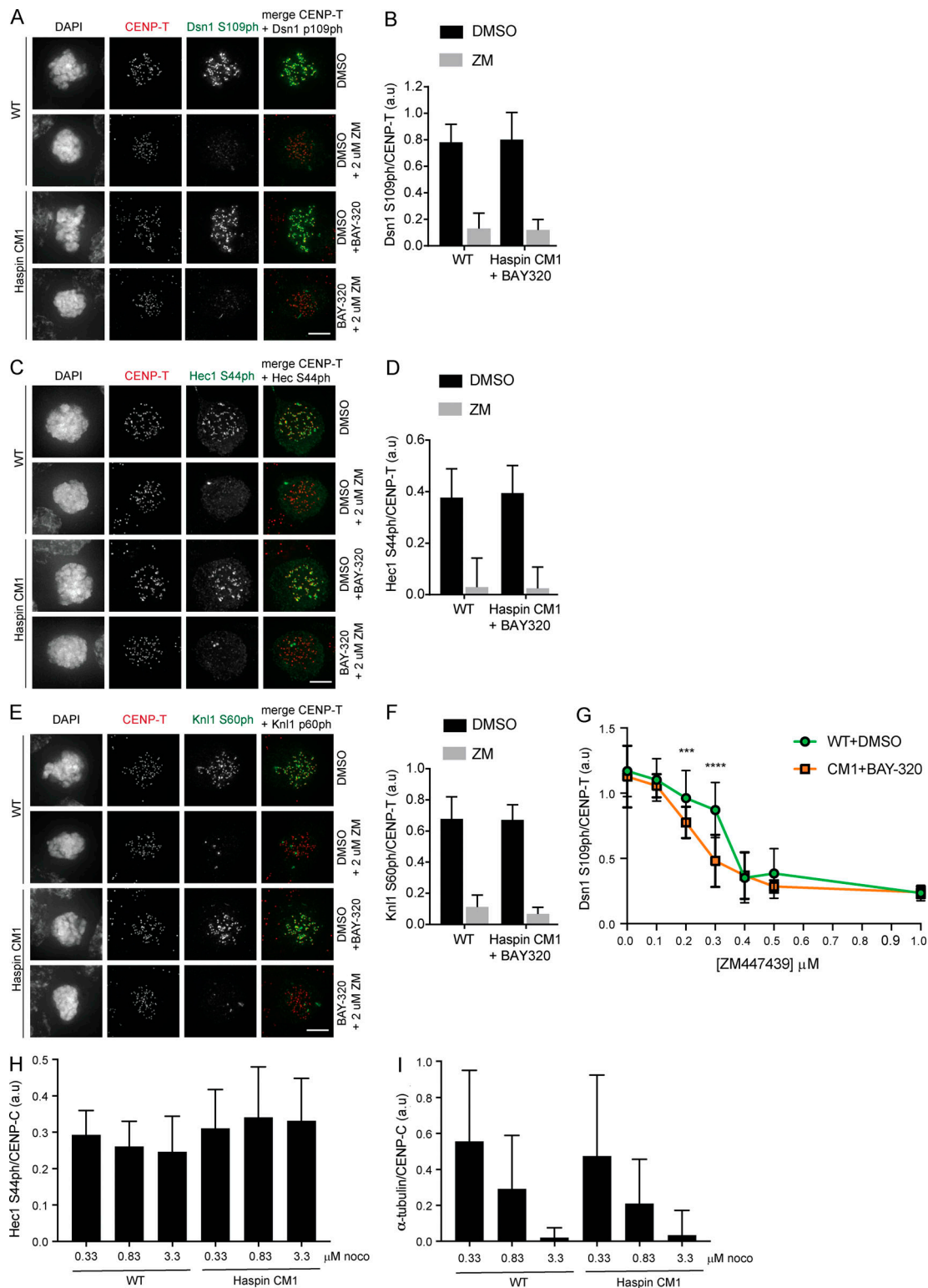
Figure S4. **IF quantification of kinetochore phosphorylation. (A–F)** IF images of HCT116 WT or Haspin CM cells ±10 µM BAY-320 in nocodazole and treated with 2 uM ZM447439 for 1 h to inhibit Aurora B kinase activity (scale bars, 5 µm). Cells were stained for Dsn1 S109ph and CENP-T (A), Hec1 S44ph and CENP-T (C), or Knl1 S60ph and CENP-T (E). IF intensity levels of Dsn1 S109ph (B), Hec1 S44ph (D), and Knl1 S60ph (F) on kinetochores. Levels were normalized over CENP-T. The graphs show the mean and SD. A minimum of 30 (Hec1 S44ph) or 21 (Dsn1 S109ph) or 19 (Knl1 S60ph) cells was quantified per condition. **(G)** HCT116 WT and HCT116 CM1 cells were blocked in mitosis by 3 h treatment with nocodazole. Subsequently, different concentrations of ZM447439 ±10 µM BAY-320 were added for 45 min, and cells were fixed. IF was performed for Dsn1 S109ph and CENP-T, and IF intensity levels at kinetochores were quantified. The graphs show the mean and SD. Statistical analysis was performed using a two-way ANOVA with Tukey's multiple comparison test. A minimum of 24 cells was quantified per condition. **(H and I)** IF intensity levels of Hec1 S44ph (H) and α-tubulin (I) on kinetochores in cells incubated with different concentrations of nocodazole for 2 h. Levels were normalized over CENP-C. The graphs show the mean and SD. A minimum of 19 cells was quantified per condition.
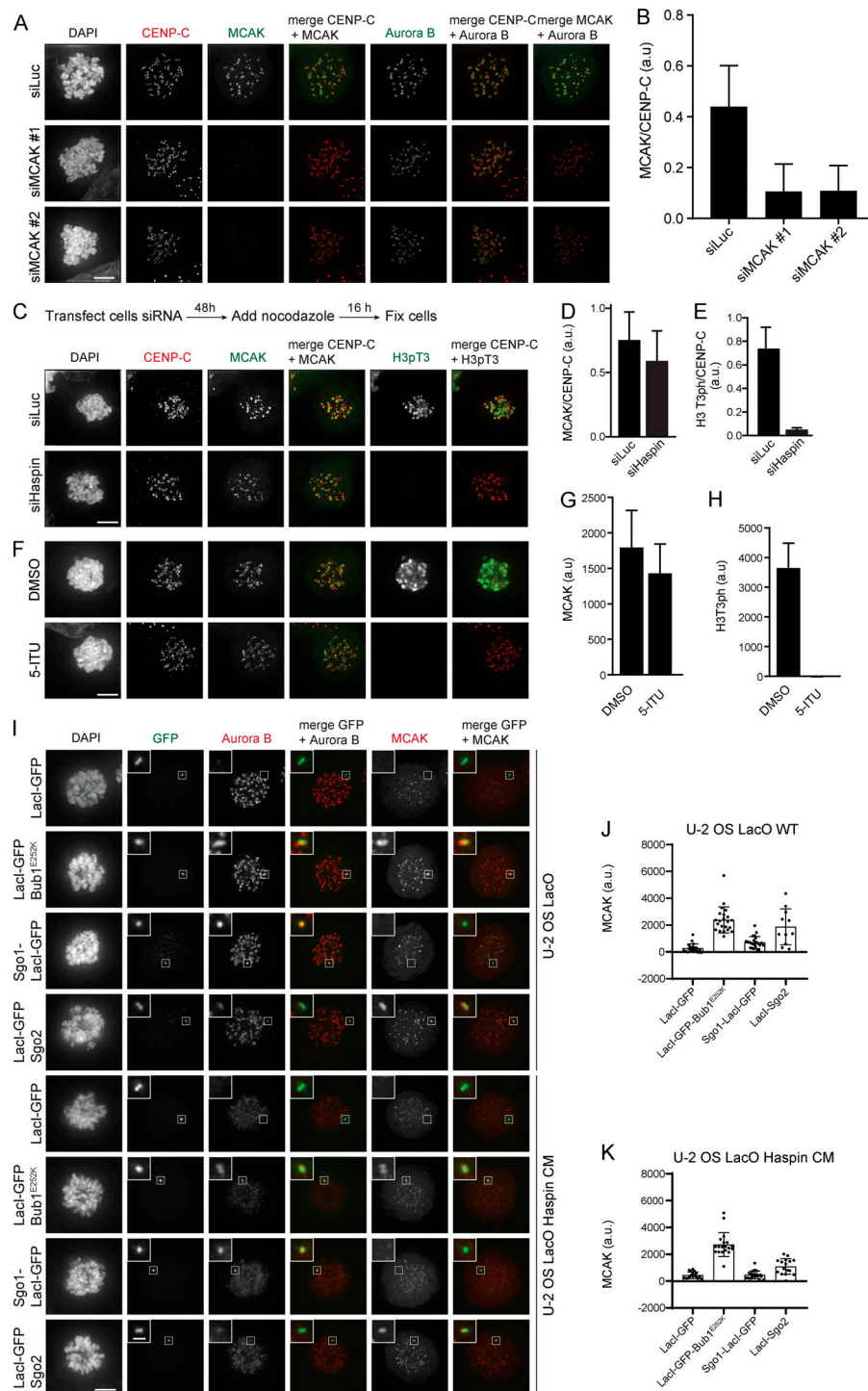
Figure S5. **Quantitative IF of centromeric MCAK. (A and B)** IF images of HCT116 WT cells transfected with siLuc or two different siRNAs targeting MCAK (scale bar, 5 μm). Cells were synchronized by a thymidine release into nocodazole and stained for MCAK, Aurora B, and CENP-C (A). IF intensity levels of MCAK at centromeres (B). Levels were normalized over CENP-C. The graphs show the mean and SD. A minimum of 20 cells was quantified per condition. **(C–E)** IF images of HCT116 WT cells transfected with siLuc or siHaspin. Cells were synchronized after 48 h by addition of nocodazole for 16 h. Cells were stained for MCAK, H3T3ph, and CENP-C (scale bar, 5 μm; C). IF intensity levels of MCAK (D) and H3T3ph (E) at centromeres. Levels were normalized over CENP-C. The graphs show the mean and SD. A minimum of 23 cells was quantified per condition. **(F–H)** IF images of HCT116 WT cells treated with 5-ITu of DMSO. Cells were synchronized by the addition of nocodazole ±2 μM 5-ITu for 2 h. Cells were stained for MCAK, H3T3ph, and CENP-C (scale bar, 5 μm; F). IF intensity levels of MCAK (G) and H3T3ph (H) at centromeres. Levels were normalized over CENP-C. The graphs show the mean and SD. A minimum of 21 cells was quantified per condition. **(I–K)** IF images of U-2 OS-LacO or U-2 OS-LacO Haspin CM cells expressing LacI-GFP, LacI-GFP-Bub1[E252K], LacI-GFP-Sgo1, or LacI-GFP-Sgo2 and arrested in mitosis using STLC (scale bar, 5 μm). The insets show the magnification of the boxed region (scale bar, 1 μm). Cells were stained for GFP, Aurora B, and MCAK. The graphs show quantifications of MCAK at the LacO array in WT (J) and Haspin CM (K) cells. Each dot represents an individual cell, and the bars indicate the mean ± SD. A minimum of 11 cells was quantified per condition.

Provided online is one table in Word. Table S1 shows genotyping of Haspin CM cell lines.